AD-A067 201 NAVAL RESEARCH LAB WASHINGTON D C F/G 20/1
THERMOSPHERIC PROPAGATION OF SONIC BOOMS FROM THE CONCORDE SUPE--ETC(U)
FEB 79 J H GARDNER, P H ROGERS

UNCLASSIFIED NRL-MR-3904 NL

END
DATE FILMED
6-79
DDC

NRL Memorandum Report 3904

Thermospheric Propagation of Sonic Booms from the Concorde Supersonic Transport

JOHN H. GARDNER

Laboratory for Computational Physics

PETER H. ROGERS

Underwater Sound Reference Division

February 14, 1979

NAVAL RESEARCH LABORATORY
Washington, D.C.

SECURITY CLASSIFICATION OF THIS PAGE (When Data Entered)

REPORT DOCUMENTATION PAGE

READ INSTRUCTIONS BEFORE COMPLETING FORM

1. REPORT NUMBER: NRL Memorandum Report 3904
2. GOVT ACCESSION NO.:
3. RECIPIENT'S CATALOG NUMBER:

4. TITLE (and Subtitle): THERMOSPHERIC PROPAGATION OF SONIC BOOMS FROM THE CONCORDE SUPERSONIC TRANSPORT.

5. TYPE OF REPORT & PERIOD COVERED: Final report

6. PERFORMING ORG. REPORT NUMBER:

7. AUTHOR(s): John H. Gardner and Peter H. Rogers

8. CONTRACT OR GRANT NUMBER(s):

9. PERFORMING ORGANIZATION NAME AND ADDRESS: Naval Research Laboratory, Washington, D. C. 20375

10. PROGRAM ELEMENT, PROJECT, TASK AREA & WORK UNIT NUMBERS: NRL Problem 77-ACE-01

11. CONTROLLING OFFICE NAME AND ADDRESS: Office of Naval Research, 800 North Quincy St., Arlington, Va 22217

12. REPORT DATE: February 14, 1979

13. NUMBER OF PAGES: 81

14. MONITORING AGENCY NAME & ADDRESS (if different from Controlling Office): 82 p.

15. SECURITY CLASS. (of this report): Unclassified

15a. DECLASSIFICATION/DOWNGRADING SCHEDULE:

16. DISTRIBUTION STATEMENT (of this Report)

Approved for public release; distribution unlimited

NRL-MR-3904

17. DISTRIBUTION STATEMENT (of the abstract entered in Block 20, if different from Report)

18. SUPPLEMENTARY NOTES

19. KEY WORDS (Continue on reverse side if necessary and identify by block number)

Sonic boom
Concorde
Thermospheric propagation
Weak shocks
Caustic

20. ABSTRACT (Continue on reverse side if necessary and identify by block number)

A nonlinear theory for the long-range propagation of sonic booms through the thermosphere has been developed. A realistic atmosphere is employed, and consideration is given to such factors as nonlinear stretching and decay of the wave, the effects of the caustic, the linear acoustic attenuation, and the increase in Mach number due to the decreasing density at high altitudes. Detailed results are presented for the case of the Concorde SST in straight, level and steady flight at 17.5 km and a velocity of Mach 2. We predict maximum ground level pressures of 0.3 Pa with an N-wave "period" of about

(Continued)

DD FORM 1 JAN 73 1473 EDITION OF 1 NOV 65 IS OBSOLETE
S/N 0102-014-6601

SECURITY CLASSIFICATION OF THIS PAGE (When Data Entered)

20. ABSTRACT (continued)

10 seconds. The sound level is a minimum along the flight track with the maximum signal strength occurring about 300 km off the flight track. The strongest received signal travels initially downward and reflects off the surface of the ocean to thermosphere. The wave turns around at an altitude of 160 km and is returned back to the ground at a horizontal distance of 320 km from the launch point. The acoustic Mach number of the wave never exceeds 0.2. Ninety percent of the wave's energy is attenuated below 100 km with 99% attenuated by the time the wave reaches the turning point.

CONTENTS

List of Symbols Used

a	attenuation factor
A	ray tube area cut by horizontal plane
A_n	normal ray tube area
$\bar{A}$	ray tube area cut by plane completely intersecting ray tube
c	speed of sound
c_n	normal phase velocity
C_p	specific heat at constant pressure
c_z	vertical phase velocity
c'	Snell's law invariant
$\bar{c}$	ray or group velocity
E	acoustic energy in a wave
f	frequency
f_L	value of f_p at transition to linear attenuation
f_p	frequency of peak spectral component of N wave
f_{peak}	frequency of peak spectral component of linearly attenuated wave
f_{rot}	rotational relaxation frequency
h_e	equivalent distance from aircraft used to compute initial N wave signature
H_s	scale height
H_1	scale height in uniform sound speed region
H_2	scale height in linear sound speed region
I_N	positive impulse of N wave

I_U	positive impulse of U wave
k	Boltzman's constant
$\bar{k}$	vertical unit vector
K_D	shape factor for directly below aircraft
K_p	atmospheric correction factor to maximum overpressure
K_s	shape factor
K_t	atmospheric correction factor to signature duration
l	distortion length by nonlinear effect
l_a	length of aircraft
m_α	mass of charged particles
M	Mach number of aircraft
M_m	mean molecular weight
n	number density
$\bar{n}$	unit vector normal to wave front
$\bar{n}'$	unit vector horizontal to wave front
p	pressure
q	perturbation velocity
q_p	maximum velocity for any phase
r	Reynolds number
$\bar{r}$	position vector
R	Gol'dberg number
s	distance along ray
t	time along ray
t_p	period of positive phase
T	absolute temperature
u	wind speed

$\bar{u}$	wind velocity
v	phase velocity of an acoustic gravity wave
U	N wave solution phase shifted through caustic
V	measure of signal strength (Blokhintsev variable) along kinematic ray
V_c	value of V behind the shock at the caustic
V_e	value of V behind the shock for an equivalent N wave
V_L	value of V behind the shock at the transition to linear attenuation
V_ω	Fourier integral transform of an N wave signature for V
V_o	value of V behind the shock at reference conditions
V_s	value of V at shock
V_+	value of V ahead of the shocks
V_-	value of V behind the shocks
$\hat{V}$	dimensionless $V = V/V_L$
$\hat{V}_{peak}$	maximum value of $\hat{V}$ for any value of the phase variable
W	integral of U
Z	altitude above sea level
α	total attenuation coefficient
α_{cl}	classical attenuation coefficient
α_{rot}	rotational relaxation attenuation coefficient
β	initial slope of N wave in expansion region
γ	ratio of specific heats
Γ	thermodynamic variable $= \frac{\rho}{c}\left(\frac{\partial c}{\partial \rho}\right) = \frac{\gamma+1}{2}\Big\|_{perfect\ gas}$
δ	sound speed gradient
Δ	perturbation from undisturbed value
η	shear viscosity coefficient
θ	inclination angle of $\bar{n}$ above horizontal

κ	thermal conductivity coefficient
λ	wave length
μ	Mach angle $= \sin^{-1}(1/M)$
ν	heading angle of wave normal $\bar{n}$
ν_a	collision frequency for scattering of charged particles by neutrals
ξ	nonlinear age variable
ξ_E	linear age variable
ρ	atmospheric density
$\sigma_{o\alpha}$	cross section of charged particles by neutrals
τ	retarded time (phase variable)
τ_c	period of N wave at the caustic
τ_e	period of equivalent N wave
τ_L	period of N wave at transition to linear attenuation
τ_s	period of N wave
τ_o	period of N wave at reference conditions
τ_1	linear phase variable
$\hat{\tau}$	dimensionless retarded time $(= \tau/\tau_L)$
ϕ	azimuthal angle of wave normal from vertical plane
x	linear age integral
ω	angular frequency
ω_b	Brunt-Vaisala frequency

Subscripts

A	aircraft
f	maximum height of ray
g	sea level

k	start of linear sound speed variation
L	transition from nonlinear to linear attenuation
o	initial value at location of emission of ray
s	shock value

THERMOSPHERIC PROPAGATION OF SONIC BOOMS FROM THE CONCORDE SUPERSONIC TRANSPORT

Executive Summary

In recent months accounts have arisen which attribute at least some of the so called "Mysterious East Coast Booms" to operation of the Concorde aircraft.[1,2] These reports differ from the conclusion of the Naval Research Laboratory investigation[3] which found that, while the Concorde was probably responsible for the booms heard in Nova Scotia, the East Coast booms were most likely caused by high performance military aircraft operating in the warning areas off the East Coast. Conjectures about Concorde induced booms have been encouraged by theories advanced by Dr. Jeremy Stone of FAS and Dr. Richard Garwin of IBM[4] involving long range propagation of the Concorde sonic boom through the thermosphere, production of superbooms, and possible adverse effects on the thermosphere. These conjectures have raised some serious questions about the nature of sonic boom propagation in the upper atmosphere. That a thermospheric mode of propagation exists is not in question. Evidence for such a propagation mode already exists and is well known.[5] However, the speculations were based on an over simplified model of sonic boom propagation and lead to a number of erroneous conclusions.

In response to a request by Dr. Frank Press, Director of the Office of Science and Technology Policy, NRL has continued its investigation and in particular looked in detail at Dr. Garwin's suggestions. In this report we describe a model which allows an accurate description of the effect produced by the portion of the Concorde sonic boom which reaches the thermosphere. We reach a number of conclusions which differ considerably from those proposed by Dr. Garwin.

Scope Of The Investigation

We consider only those sonic booms which are refracted to the ground by the sound velocity gradient in the thermosphere. That is, we consider only those waves which reach an alti-

Manuscript submitted December 4, 1978.

tude of more than 100 km before curving downward and returning to earth. We consider both the sonic boom which propagates directly to the thermosphere and the boom which, while initially traveling downward, reflects off the water and returns to the thermosphere. We recognize that off the flight track the sonic booms can also be returned to the ground by winds in the stratosphere, usually from a height of about 50 km. These stratospheric returns have been studied by the British[6] and are believed to be the cause of the "bumps in the night" heard in England. This propagation mode is well understood and shall not be considered in this report.

We use a realistic model for the atmosphere but do not take into account the details of the wind-temperature structure. The reason for limiting the problem in this manner is that the atmospheric structure depends on the time of day, the season, the state of solar activity, latitude, weather etc.,[7] the variability of which render consideration of the detailed structure practically meaningless. We rather aim towards obtaining both typical and worst case results.

We consider only the case of the aircraft in straight, level, and steady flight. We recognize that it may be possible for a upward going sonic boom to focus at the ground for a decelerating or turning aircraft. Such a focus, however, would occur over only a small area on the ground and, in any case, would result in ground pressure levels which would exceed our predictions by no more than a factor of three.

We include in our theory the variation with altitude of sound speed, density, and pressure resulting from a realistic model of the atmosphere. We also include the nonlinear stretching and decay of the wave, the focussing which occurs at the caustic near the turning point, the effects of linear acoustic attenuation, and the effects of winds. From our model, we determine the boom strength as a function of altitude and the ground pressure both on and off the flight track. We have studied, and determined to be unimportant, gravity wave effects, strong shock effects, plasma effects, and the effects of a finite mean free path.

Results And Conclusions

We have developed a model for thermospheric propagation of the sonic boom from a Concorde aircraft. The model, which is for the most part analytic, accounts for all the physical effects which we believe to produce a significant effect on the result. Based on the results obtained from this model, we reached the following conclusions:

1. The ratio of boom pressure to undisturbed pressure in the thermosphere never exceeds 0.2. This confirms the validity of our weak shock model and implies that no large perturbations (such as high temperatures which might produce strange lights) of the thermosphere will occur.

2. Over 90% of the sonic boom's energy is lost before it reaches 100 km. There is, therefore, insufficient energy remaining in the wave to cause winds nearly as large as those which naturally occur in the thermosphere.

3. The sonic boom will reach the ground at a horizontal distance of about 320 km from the point it left the aircraft.

4. Along the flight track, the Concorde, if it remains in straight and level flight, will pass over head approximately 13 minutes before the first arrival of the boom from the thermosphere. The average horizontal velocity of the sonic boom is less than half that of the Concorde in cruise mode. It is thus highly unlikely that there could exist reasonable conditions of aircraft deceleration under which the boom would precede the aircraft.

5. The sound received along the flight track is a minimum. The largest signals occur 200 to 400 km from the flight track.

6. The largest signals are produced by the initially downward boom which reaches the thermosphere by first reflecting from the ocean.

7. The sound received will in all cases be small (less than .5 Pa) and very low in frequency (approximately .1 Hz).

We conclude that thermospheric returns from Concorde are of sufficiently low amplitude and frequency that it is unlikely that they are either responsible for the East Coast events or likely to disturb the public. In addition, we conclude that the sonic boom from the Concorde does not have sufficient amplitude or energy to produce a deleterious effect on the thermosphere.

1. Geometric Acoustics, Snell's Law and Blokhintsev Invariance

The propagation of weak sound waves in the atmosphere under a limited number of assumptions is governed by the theory of geometric acoustics. This is a special case of the more general geometric theory of general linear wave propagation. A general theory for non-dissipative waves may be derived (see for instance Hayes[8]) which is an asymptotic theory for a slowly varying, nonuniform medium for which the local solutions are very close to those obtained for plane waves. The theory is asymptotic in the sense that it requires the wave number to be large in some relative sense. For example, the wave length must be small compared to the scale length of the inhomogeneities in the atmosphere. If, in addition, the waves are nondispersive, arbitrary functions of some phase variable may be used to describe a general wave signature. A linear, inviscid, acoustic theory leads to a geometric theory which is nondissipative and nondispersive. The geometric theory allows the partial differential equation for the wave fronts to be reduced to the integration of a set of ordinary differential equations along the characteristics. It also provides a means of describing the kinematics of the solution independent of the dynamics. Thus, from different orders of the asymptotic expansion, we obtain solutions for the ray paths and wave front curvature and an energy invariant rule which allows the calculation of the wave amplitude. The equations for the ray path and wave front vector given for geometric acoustics are: (see for example Hayes et al).[9]

$$\frac{d\bar{r}}{dt} = \bar{c} = c\bar{n} + \bar{u} \tag{1-1}$$

$$\frac{d\bar{n}}{dt} = \nabla c + (\nabla \bar{u})\cdot\bar{n} - \bar{n}\,[\bar{n}\cdot\nabla c + \bar{n}\cdot(\nabla \bar{u})\cdot\bar{n}] \tag{1-2}$$

where $\bar{r}$ is the ray, c the local sound speed, $\bar{u}$ the wind vector, and $\bar{n}$ the wave front normal. For the case of a stratified medium this equation possesses a first integral which yields Snell's law (see Ref. 9). In simple terms, this law states that the horizontal vector component of the inverse phase velocity $\frac{\bar{n}}{c_n}$ is a constant along rays. That is,

$$\frac{\cos\theta\ \bar{n}'}{c_n} = \text{const.} \tag{1-3}$$

where

$$\bar{n} = \cos\theta\bar{n}' + \sin\theta\bar{k}$$
$$c_n = \bar{c}\cdot\bar{n} = c + \bar{u}\cdot\bar{n} \quad .$$

The second order term of the expansion in reciprocal wave number leads to an energy invariance law. This is equivalent to the definition of an adiabatic invariant for the wave propagation. Restricted to the validity of geometric acoustics, an invariant law was found by Blokhintsev, which is valid for an atmosphere with steady winds[10]. This result has been extended to be valid for unsteady medium by Garret[11] and Hayes,[12] but this has little application to the problem at hand and is difficult to implement. The basic result is that an invariant is found which is the product of the Rayleigh acoustic energy density ρq^2 and the ratio of the local phase velocity to the local sound speed c_n/c. The product of the invariant quantity times the volume flow is then a constant along a kinematic ray defined earlier.

$$\rho q^2 \frac{c_n}{c}\ \bar{c}\cdot\bar{A} = \text{const.} \tag{1-4}$$

We choose to express this invariance following Hayes et al[9] as a constant c' times the square of a variable V

$$c'V^2 = \frac{\rho q^2}{c}\ c_n\bar{c}\cdot\bar{A} \tag{1-5}$$

$\bar{c}$ is the group velocity defined earlier and $\bar{A}$ is any cross section which completely cuts the ray tube. This then provides the basis by which the amplitude of the wave can be computed along a ray path knowing the amplitude anywhere along the ray path. If, as is convenient for a hor-

izontally stratified atmosphere, we take A to be the area cut by a plane of constant z, then $\bar{c}\cdot\bar{A} = c_z A$. From Snell's law the result can be obtained that $c_z = c \sin\theta$ and $c_n = c' \cos\theta$. This gives our conservation variable as:

$$I = \sqrt{\rho c^2 A \sin\theta \cos\theta}\left(\frac{q}{c}\right). \tag{1-6}$$

The disturbance Mach number (q/c) is a measure of the strength of the signal. The problem is completely determined once the ray tube area A is computed. This can be done by quadrature once the solution for the rays is known.[9,12] The theory as it stands is a completely linear one. This leads to physically incorrect results as we shall see later.

2. Linearized Lossless Approach (Garwin)[4]

As long as the linear theory of geometric acoustics remains valid, the Blokhintsev invariance allows signal strength to be calculated for an arbitrarily varying inhomogeneous atmosphere as long as it remains steady. We may use this invariance to estimate the signal strength for a supersonic aircraft such as the Concorde at the altitude where the rays turn over. For simplicity, let us assume there are no winds and assume a simple cylindrical spreading of the wave so that the ray tube area is proportional to the distance travelled. It can be shown for a horizontally stratified atmosphere that this distance is the horizontal distance if we are looking along the flight track. We are neglecting the focussing of the wave near the caustic, an unnecessary complication at this stage. The invariant is then

$$c' V^2 = \rho q^2 \, cA_n = \frac{\Delta p^2}{\rho c} A_n = \text{const} \tag{2-1}$$

where $\Delta p = \rho c q$ when geometric acoustics is valid. If we use the atmosphere described in the model atmosphere section, we find that for an $M = 2$ aircraft at 17.5 km, the altitude at which the phase velocity equals the aircraft speed is about 160 km. The ray path found from using the model atmosphere extends about 150 km horizontally to the turnover point. If we use Dr. Garwin's estimates for the boom strength of 100 Pa at 25 km, we can calculate the boom strength at 160 km. However, the more interesting number is the ratio of the acoustic energy to the local ambient energy density since this is a measure of relative boom strength. To get this, we observe that

$$\frac{\Delta p^2}{\rho c} A_n = \frac{\Delta p^2}{\gamma p^2} pcA_n = \text{const.} \tag{2-2}$$

Thus, the ratio of $(\Delta p/p)^2$ at 160 km compared to the value on the ground is given by

$$\frac{(\Delta p/p)^2_{160}}{(\Delta p/p)^2_g} = \frac{(pcA)_g}{(pcA)_{160}} = \left[\frac{p_g}{p_{160}}\right]\left[\frac{c_g}{c_{160}}\right]\left[\frac{A_g}{A_{160}}\right] \tag{2-3}$$

The ratios for this example are given by: $p_g/p_{160} = 3.7 \times 10^8$, and $c_g/c_{160} = 0.5$, where $A_g/A_{160} = \frac{25}{150} = 1/6$, yielding a ratio of $\frac{(\Delta p/p)^2_{160}}{(\Delta p/p)^2_g} = 3 \times 10^7$. This represents a very large increase in the strength of the wave which would completely invalidate the geometrical acoustic theory. As we shall see in the next section, there are other factors which become important rendering the above simple estimate invalid.

This result is similar to Dr. Garwin's argument[4] when he postulated strong shocks and large temperature rises in the thermosphere. In his approximation he used $A_g/A_{180} = \frac{25}{500} = .05$ but assumed $c_g/c_{180} = 1$. Also he used $p_g/p_{180} = 10^9$ giving a result that $\frac{(\Delta p/p)^2_{180}}{(\Delta p/p)^2_g} = 5 \times 10^7$ which differs little from the estimate given above. The critical assumption in the above estimates is that the wave will propagate to the thermosphere *as a linear wave*. This is not true even for weak waves as we shall see in the next section.

3. Nonlinear Analysis

The analysis in the previous section was based on a linear geometrical acoustic theory used to derive ray equations and an energy invariant law. It is well known, however, that acoustic signals distort when propagating over long distances. This distortion is caused by a weak, nonlinear effect resulting from small changes in propagation speed which are proportional to the local strength of the disturbance. Although the nonlinear effect is locally weak (an assumption that must be true for geometric acoustics to be valid), it is cumulative and the distortion of a signal which has propagated over a long distance may be far from small.

In order to simplify the analysis, we make the usual assumption that to lowest order the phase shift of the wave due to the change in propagation speed is the only nonlinear effect considered. Hayes[13] has shown that for the case of level flight in a uniform atmosphere, the error corresponds to a higher order term in a small parameter. The assumption of a single nonlinear effect should be valid as long as geometric acoustics is valid and as long as the disturbances are weak. The problem of the nonlinear effect on rays has been considered by Whitham[14,15,16] for finite strength shocks.

The effect of the small disturbance on the propagation velocity is to change the group velocity from $\bar{c} = c\bar{n} + \bar{u}$ in the undisturbed fluid to $\bar{c} = (c + q)\bar{n} + \bar{u}$. The change in the speed of sound is given by $\Delta c = (\Gamma - 1)\,\frac{\Delta p}{\rho c} = (\Gamma - 1)q$ where Γ is a thermodynamic quantity defined by $\Gamma - 1 = \frac{\rho}{c}\left(\frac{\partial c}{\partial \rho}\right)_s$. The change in propagation velocity is given by $\Gamma q\bar{n}$. The phase shift expressed as a distance from the linear wave front is given by

$$\frac{dl}{dt} = -\Gamma q$$

where t is the time along the ray and l is the local displacement. The local displacement is related to the phase by $dl = c_n d\tau$ where τ is a phase variable. Thus,

$$\frac{d\tau}{dt} = -\Gamma \frac{q}{c_n} \tag{3-1}$$

Integrating Eq. (3-1) yields the phase shift of the nonlinear signal.

The linear theory gives the result that for the Blokhintsev invariant

$$\left.\frac{\partial V}{\partial t}\right|_{\tau} = 0 \tag{3-2}$$

That is, along the linear characteristics, the quantity V = constant. If we define a phase variable $d\tau = dt - \frac{dl}{c_n}$ where $dl\bar{n} = d\bar{r}$, then the effect of the nonlinearity can be included with an extra term proportional to the phase shift giving an inviscid Burgers' equation:

$$\frac{\partial V}{\partial t} = \frac{\Gamma q}{c_n} \frac{\partial V}{\partial \tau} \tag{3-3}$$

If we now use the definition of V to relate it to $\frac{\Gamma q}{c_n}$ and if we introduce an "age" variable defined by

$$\xi = \int \frac{\Gamma dt}{c_n(\rho A \sin\theta \cos\theta)^{1/2}} \tag{3-4}$$

then the equation becomes a simple expression with the independent variables "age" and retarded time (or phase). Thus,

$$\frac{\partial V}{\partial \xi} = V \frac{\partial V}{\partial \tau} \tag{3-5}$$

This equation has an analytic solution in terms of the linear phase variable τ_1. The phase shift is given by $\frac{d\tau}{d\xi} = -V(\tau, \xi)$. Now if we assume that the Blokhintsev invariance and ray tube area are unaffected by the phase shift (an assumption we justified earlier), then we have $V(\tau, \xi) = V(\tau_1)$ where τ_1 is the linear phase and τ the actual phase. The solution of the

phase shift equation gives $\tau = \tau_1 - \xi V(\tau_1)$. The linear phase τ_1 is then a function of τ and ξ. The solution of this equation may become multivalued in τ. This can be resolved by taking into account the presence of shock waves.

The distortion of an arbitrarily shaped signal is depicted in Figure 3-1. The rate of distortion is proportional to the amplitude of the wave for any value of the phase variable. Assuming Blokhintsev invariance, the amplitude of the signal remains unchanged. Thus, the portion of the signal with large amplitude will tend to overrun the region ahead of it with smaller amplitude until the solution becomes multivalued. This multivaluedness may be removed by fitting shocks to the solution rendering it single valued. For weak shocks it can be shown that the shock speed is equal to one half the sum of the characteristic speed in front of and behind the shock.[17] This leads to the relation

$$\left.\frac{d\tau}{d\xi}\right|_{SHOCK} = -\frac{1}{2}(V_+ + V_-) \tag{3-6}$$

This can also be shown to be equivalent to the equal area rule[18] which says that the integral of the solution with respect to phase τ with the shock fitted should give the same area as the multivalued solution for each lobe of the solution. This is also equivalent to assuming the existence of a velocity potential which is continuous across shocks. Again shocks are located so that the integral of the wave with and without shocks gives the same result.

As shown in Figure 3-1, as the signal distorts further, shocks tend to overrun one another and eat up the entire solution until the asymptotic form of the pulse forms an N wave (which is characteristic of the far field solution) with two shocks separated by a linear expansion region. This form of the solution will always be arrived at for a sufficiently large "age" parameter.

In the case of an N wave, there exists a particularly simple analytic solution to the fitting of shock waves. The solution for the linear part of the wave is given by

$$V = \frac{-\beta\tau}{1 + \beta\xi} \tag{3-7}$$

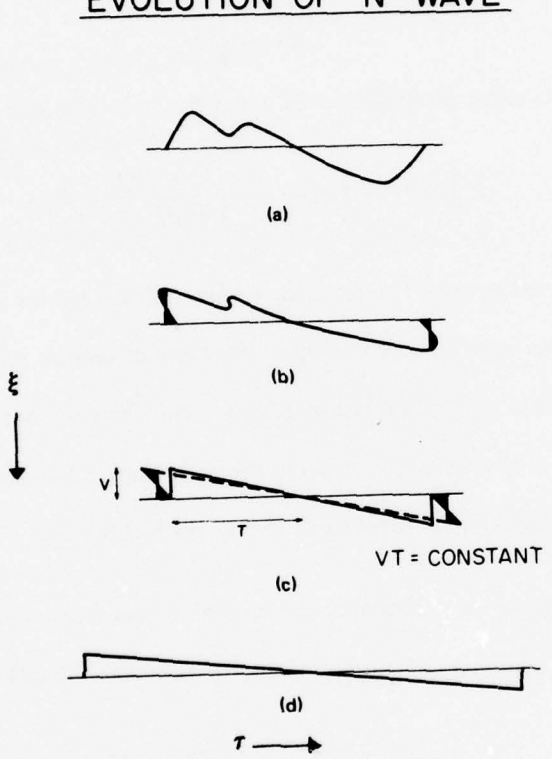

Fig. 3.1 — Evolution of a near field to a far field signature. Larger amplitude parts of the waveform propagate faster overtaking lower amplitude parts and forming shocks. Shocks are fitted keeping total area under a lobe constant.

The bisector rule gives the velocity of the leading shock as:

$$\left.\frac{d\tau}{d\xi}\right|_{SHOCK} = -\frac{1}{2} V_s = \frac{1}{2} \frac{\beta\tau_s}{1+\beta\xi} \tag{3-8}$$

This can be integrated to give

$$\tau_s = \tau_o(1+\beta\xi)^{1/2} \tag{3-9}$$

From the initial conditions at $\xi = 0$, we get

$$\beta = -\frac{V_o}{\tau_o} \tag{3-10}$$

This solution gives, as required, that the area under the front half lobe is conserved.

$$2\int_{\tau_s}^{0} V d\tau = V_s\tau_s = \frac{V_o\tau_o(1+\beta\xi)}{1+\beta\xi} = V_o\tau_o \tag{3-11}$$

The error involved in using the far field N wave solution for the entire path involves only the period of aging the wave into an N profile. For cases of upward propagation, where the age becomes very large, this takes place rather quickly. The error involved would be a somewhat enhanced dissipation of the wave by shocks in the early part of the calculation. An equivalent N wave for a given F function for the aircraft can always be obtained.

In order to complete the solution to the inviscid Burgers' equation, we must evaluate the "age" integral for ξ as a function of position along the ray paths. Recall that

$$\xi = \int \frac{\Gamma dt}{c_n (\rho A \sin\theta \cos\theta)^{1/2}} \tag{3-12}$$

From Snell's law we have that

$$\frac{dz}{dt} = c \sin\theta$$
$$c_n = c' \cos\theta \tag{3-13}$$

Initially, so that the integrals will be reasonably simple and analytically tractable, we make a few simplifying assumptions. One is that there are no winds, and the second is that only rays

along the flight track will be considered. Later we will dicsuss how to remove these restrictions at the expense of complicating the integrals. With no winds, $c = c' \cos\theta$ and

$$\xi = \frac{\Gamma}{c'^2} \int \frac{dz}{\sin\theta \cos^2\theta \, (\rho A \sin\theta \cos\theta)^{1/2}} \tag{3-14}$$

Our model atmosphere, discussed in section four, has postulated two separate parts to the ray path. In the lower region, up to a break point altitude, the sound speed is held constant yielding straight ray paths at the initial inclination angle. The second part consists of a region where the sound speed increases linearly with altitude yielding ray paths which are arcs of a circle. The radius is determined by the sound speed gradient. It is natural then to break the "age" integral into two parts corresponding to these two different ray paths. For altitudes below the break point, only the first part of the integral applies, with the upper limit set to the altitude in question.

The density formulas are given in the section describing the atmosphere. The remaining unknown, the ray tube area, is discussed below. The dimensions of the ray tube area are completely arbitrary as they appear only as a ratio in all of the formulas. These areas may be found by quadrature once the rays have been found.[9] The formula for rays along the flight tracks for a plane moving in steady level flight is (see Hayes et al[9])

$$A = \frac{\sin\theta_o}{\cos\theta_o} \int_Z \frac{\cos\theta}{\sin\theta} \, d(-Z) \tag{3-15}$$

The rays are given in two segments. The first has $\cos\theta$ and $\sin\theta$ constant. In the second region $\cos\theta = \cos\theta_o[1 + \delta (Z - Z_k)]$ which is the Snell's law solution for a linear sound speed profile. Thus:

$$A = \begin{cases} Z & \text{for } Z < Z_k \\ Z_k + \dfrac{\sin\theta_o}{\delta \cos^2\theta_o} [\sin\theta_o - \sin\theta] & \text{for } Z_k < Z < Z_f \end{cases} \tag{3-16}$$

At this time, a transformation of variables is convenient. We introduce:

$$\zeta = \frac{Z - Z_A}{2H_1} \text{ and } \frac{1}{\eta} = \cos\theta = \cos\theta_o \left[1 + \delta\,(Z - Z_k)\right] \tag{3-17}$$

After considerable algebraic manipulation, we get

$$\xi = \frac{\Gamma\, e^{-\zeta_o}\,(2H_1)^{1/2}}{c'^2\,\rho_o^{1/2}\,(\sin\theta_o)^{3/2}\,(\cos\theta_o)^{5/2}} \left[\int_{\zeta_o}^{\zeta_k} \frac{e^{\zeta}}{\sqrt{\zeta}}\, d\zeta + \frac{\sin\theta_o\,(\cos\theta_o)^{3/2}\, e^{\left(\zeta_1 + \frac{1}{2H_2\delta}\right)}}{\sqrt{2H_2\,\delta}} \cdot \right.$$

$$\left. \int_{\frac{1}{\cos\theta}}^{\frac{1}{\cos\theta_o}} \frac{\eta^{3/2}\, e^{-\frac{\cos\theta_o}{2H_2\,\delta}\,\eta}\, d\eta}{(\eta^2 - 1)^{3/4} \left[\left(\frac{\delta\cos^2\theta_o}{\sin\theta_o} Z_1 + \sin\theta_o \right) \eta - \sqrt{\eta^2 - 1} \right]^{1/2}} \right] \tag{3-18}$$

The integral to be evaluated in the "isothermal" region below Z_k is of the form

$$I_1(\zeta) = \int \frac{e^{\zeta}}{\sqrt{\zeta}}\, d\zeta \tag{3-19}$$

This is Dawson's integral[19] which cannot be further reduced. The function is tabulated or can easily be evaluated from its power series

$$I_1(\zeta) = 2\,\zeta^{1/2} \sum_{n=0}^{\infty} \frac{\zeta^n}{(2n+1)\,n!} \tag{3-20}$$

The integral to be evaluated above Z_k is of the form

$$I_2(\eta_i) = \int_{\eta_i}^{1/\cos\theta_o} \left\{ \frac{\eta}{(\eta+1)^{3/4} \left[1 - \frac{(\eta^2-1)^{1/2}}{D\eta} \right]^{1/2}} \right\} \frac{e^{-B\eta}}{(\eta-1)^{3/4}}\, d\eta \tag{3-21}$$

where η_i will vary from 1 (when $Z = Z_f$) to $\frac{1}{\cos\theta_o}$ (when $Z = Z_k$). Of most interest is the case when $\eta_i = 1$, in which case the integrand has an integrable singularity at the end point. The analysis must properly account for this singularity.

The most significant contributions to the integral come from smaller values of η where the exponential and $(\eta - 1)^{-3/4}$ terms dominates. We rewrite I_2 as

$$I_2(\eta_i) = \int_{\eta_i}^{\frac{1}{\cos\theta_o}} \frac{G(\eta)}{(\eta - 1)^{3/4}} e^{-B\eta} d\eta \tag{3-22}$$

where

$$G(\eta) = \frac{\eta}{(\eta + 1)^{3/4}\left[1 - \frac{(\eta^2 - 1)^{1/2}}{D\eta}\right]^{1/2}} \tag{3-23}$$

$G(\eta)$ is slowly varying except near $\eta = 1$ where $[1 - \frac{(\eta^2 - 1)^{1/2}}{D\eta}]^{1/2}$ has an infinite derivative. To isolate the effect of the infinite slope, we subtract from $G(\eta)$ the quantity $(\eta - 1)^{1/2}/(2D\ 2^{3/4})$. Its derivative has the same limit as that of $G(\eta)$ as $\eta \to 1$. Hence,

$$I_2(\eta_i) = \int_{\eta_i}^{1/\cos\theta_o} \frac{F(\eta)\ e^{-B\eta}}{(\eta - 1)^{3/4}} d\eta + \frac{F(1)}{2D} \int_{\eta_i}^{1/\cos\theta_o} \frac{e^{-B\eta}}{(\eta - 1)^{1/4}} d\eta \tag{3-24}$$

where

$$F(\eta) = G(\eta) - \frac{(\eta - 1)^{1/2}}{2\ D\ 2^{3/4}} . \tag{3-25}$$

The function $F(\eta)$ is slowly varying over the entire range of possible values for η, $1 \leqslant \eta \leqslant 2$. We can therefore, to a good approximation, replace $F(\eta)$ by the straight line

$$F(\eta) = F(1) + 2\left[F(\tfrac{3}{2}) - F(1)\right](\eta - 1) \tag{3-26}$$

which is exact at $\eta = 1$ and $\eta = 3/2$. Equation (3-24) becomes

$$\begin{aligned} I_2(\eta_i) = {} & F(1) \int_{\eta_i}^{1/\cos\theta_o} \frac{e^{-B\eta}}{(\eta - 1)^{3/4}} d\eta \\ & + \frac{F(1)}{2q} \int_{\eta_i}^{1/\cos\theta_o} \frac{e^{-B\eta}}{(\eta - 1)^{1/4}} d\eta \\ & + 2\left[F\left\{\frac{3}{2}\right\} - F(1)\right] \int_{\eta_i}^{1/\cos\theta_o} (\eta - 1)^{1/4} e^{-B\eta} d\eta . \end{aligned} \tag{3-27}$$

The integrals in Eq. (3-27) can be evaluated exactly in terms of the incomplete gamma functions

$$I_2(\eta_i) = \frac{e^{-B}}{B^{1/4}} \left[F(1)\ \Gamma\ (1/4,\ B\eta) + \frac{F(1)}{2DB^{1/2}}\ \Gamma\ (3/4,\ B\eta) \right. \tag{3-28}$$
$$\left. + \frac{2[F(3/2) - F(1)]}{B}\ \Gamma\ (5/4,\ B\eta) \right]_{\eta = \eta_i}^{\eta = 1/\cos\theta_0}$$

The incomplete gamma functions $\Gamma\ (1/4,\ B\eta)$ and $\Gamma\ (3/4,\ B\eta)$ can be evaluated using either the power series or the continued fraction representations. $\Gamma\ (5/4,\ B\eta)$ can be expressed as a sum of $\Gamma\ (1/4,\ B\eta)$ and an exponential.[20] Equation (3-28) agrees with the numerical integration of Eq. (3-21) to within 2% for all values of η_i.

If we wish to consider winds, then we no longer get a simple relation between sound speed and cos θ. Snell's law gives the result that

$$\cos\theta = \frac{c}{c' + u} \tag{3-29}$$

If the wind speed u is a constant, then the simple law applies. We can get a lowest order approximation to the effect of wind by assuming the wind to be zero in the lower region and equal to a constant in the linear sound speed region. This gives a discontinuity in the ray slope which violates the assumption of geometric acoustics. What actually happens is that the wave will be partially reflected from this discontinuity. If the discontinuity is small, then the reflected part will be small. The solution we obtain, in any case, overestimates the signal strength and thus gives an upper bound.

If we wish to consider rays other than along the flight tracks, the area formulas must be modified. The complication is not too severe if we require the winds to be zero for these cases. Then the area formula is (see Ref. 9)

$$A = \left(\frac{\sin \mu}{\cos \theta_{\infty}} + \frac{\sin^2 \phi}{\cos^2 \phi} \frac{1}{\cos \theta_{\infty} \sin \mu} \right) \int_{\ell} d(-Z) +$$

$$+ \frac{\sin \mu}{\cos \theta_{\infty}} \frac{\sin \theta_{\infty}}{\cos \theta_{\infty}} \int_{\ell} \frac{\cos \theta}{\sin \theta} d(-Z)$$

$$+ \frac{c_{\infty}^2 \sin^2 \phi}{\sin \mu} \frac{\sin \theta_{\infty} \cos^2 \mu}{\cos^4 \theta_{\infty}} \int_{\ell} \frac{1}{c^2} \frac{\cos^3 \theta}{\sin^3 \theta} d(-Z). \tag{3-30}$$

Using Snell's law and integrating yields

$$A = \left(\frac{\sin \mu}{\cos \theta_{\infty}} + \frac{\sin^2 \phi}{\cos^2 \phi} \frac{1}{\cos \theta_{\infty} \sin \mu} \right) Z$$

$$+ \frac{\sin \theta_{\infty}}{\alpha \cos^2 \theta_{\infty}} \left(\frac{\sin \mu}{\cos \theta_{\infty}} + \frac{\sin^2 \phi}{\cos^2 \phi} \frac{\sin \theta_{\infty}}{\cos \theta_{\infty} \sin \mu} \frac{1}{\sin \theta} \right) (\sin \theta_{\infty} - \sin \theta). \tag{3-31}$$

The angle ϕ is the azimuthal angle the ray makes with the vertical and $\mu = \sin^{-1}(1/M)$ is the Mach angle. From the relation

$$\sin \theta_o = \cos \mu \cos \phi \tag{3-32}$$

the angle θ_o can be determined for a given Mach number and azimuthal angle ϕ. The heading of the ray with respect to the flight track can be computed from the relation

$$\tan \nu = \sin \phi \cot \mu \tag{3-33}$$

The general formulas are given in Reference 9. We have considered only the limited cases of straight, level, and steady fight to simplify the integrals. The more general formulas would require a numerical calculation. Estimates of the primary effects we seek can be found, however, from these simpler relations.

Examining the integral for the age, we note that the biggest variation in the integrand is due to the exponentially decreasing density with altitude. Thus, the largest part of the contribution to the integral will come from the region of lowest density near the top of the ray path. Examining Figure 3-2 which shows a plot of log density along the ray path, we see that the greatest part of the path is in the region of lowest density. For this reason, the aging of the wave takes place almost entirely near the top of the ray path.

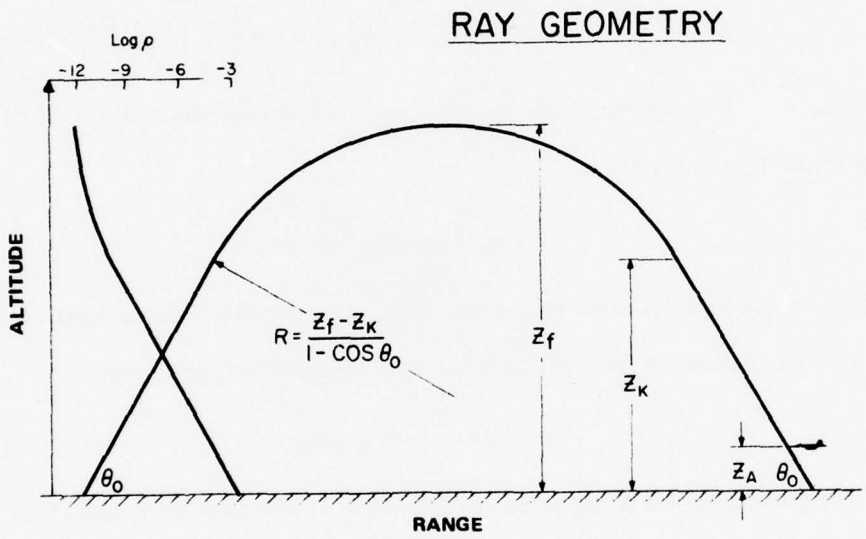

Fig. 3.2 — Ray path along ground track for model atmosphere. Note that a disproportionate amount of the path is in a region of low density causing most of the "aging" to occur at high altitudes.

4. Atmospheric model

The ray paths are determined by the sound speed and wind profiles in the atmosphere. The altitude at which the ray turns over is determined by where the phase velocity (sound plus wind speed) is equal to the aircraft speed (if we assume no winds at the aircraft altitude). Below 20 km, data for the temperature and wind velocity are routinely taken by the weather service. Sounding rocket data has provided good, seasonally averaged data for altitudes up to 50 km. Above 50 km the wind data is scarce and many of the wind profiles must be inferred from models of the thermosphere and upper stratosphere. In the regions above 20 km, where daily weather data is unavailable, there may be considerable daily variation in the winds due to tidal effects. In regions above 100 km the variations exceed the mean values so that no reliable wind data for a given time is available. Wind speeds of the order of 100 m/s are found at 125 km and decrease to around 50 m/s at 150 km.[7] Since no predictive capability seems reasonable based on these wind variations, it was felt best to ignore the wind effect except to determine worst case results based on known maximum winds. Otherwise, the results were computed ignoring the effect of winds. Measurements of the temperatures and density profiles have been more extensive in the upper atmosphere, and a number of models exist that predict temperature and specie density as a function of altitude. In the region above 120 km the temperature and density profiles are strongly influenced by the solar flux of energy into the thermosphere. Variations of several hundred degrees exist between the maximum daytime and nighttime exospheric temperature. The minimum exospheric temperature, which is also used in determining the maximum temperature, is also a function of solar activity. These temperatures are also a function of latitude and time of day. It is possible, therefore, to generate a very large parameter range of temperature and wind profiles which will alter the ray paths and, most importantly,

the maximum altitude of the ray. We have chosen to find solutions for a reasonable set of parameters and then investigate how these solutions might independently vary with the parameters.

Models exist which can predict the temperature and specie concentrations for a given solar activity, latitude, and time of day. The JACCHIA '71[21] model is the one we are currently using. To narrow the problem somewhat, we have chosen a solar flux for December 2, 1977 as a representative value. This also corresponds to one of the "event" days. We chose a latitude of 41°N and a time of 12 noon to correspond to Concorde arrival in New York.

The important parameter that the models predict in terms of the ray paths is the local sound speed rather than the temperature. At altitudes above 100 km the composition of the atmosphere changes resulting in a lower mean molecular weight. This has the effect of raising the sound speed for a given temperature since $c^2 = \frac{\gamma nkT}{M_m}$. This can increase the sound speed by as much as 20% more than that obtained using a constant mean molecular weight atmosphere at 180 km. This effect lowers the peak altitude of the ray by 20 km.

In Figure 4-1 we show a comparison of the JACCHIA '71 model sound speed compared to the U.S. 1976 Standard Atmosphere profile.[22] The results are similar enough that either could be used. We use the JACCHIA '71 model results for the calculations presented here.

In order to make our calculations analytically integrable, we have chosen to make another simplification of the atmospheric model. We construct a model atmosphere that has a constant sound speed up to some turning point Z_k and then a linear increase in the sound speed up to the altitude Z_f where the ray reaches its maximum altitude. The constant sound speed is equal to the sound speed c_o(295 m/s) at the Concorde cruise altitude. The point Z_k (103 km) is the

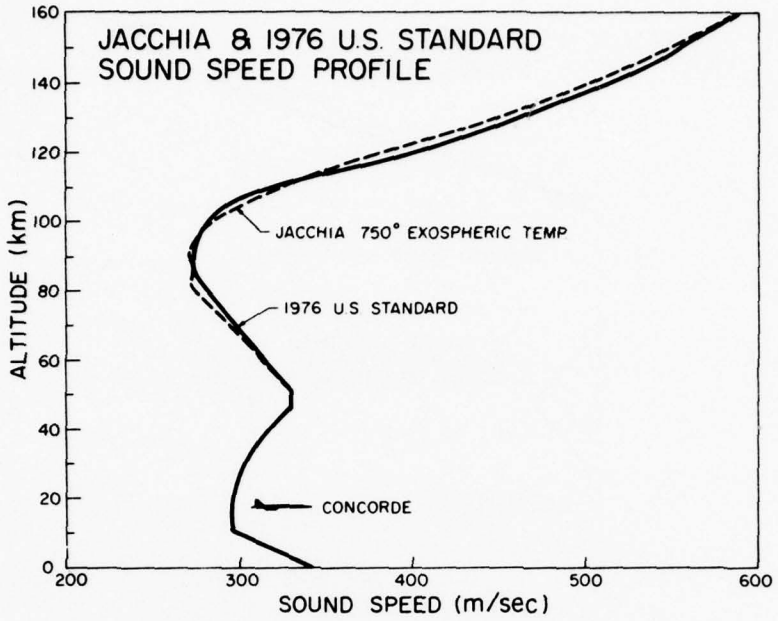

Fig. 4.1 – Comparison of the sound speed from the Jacchia model atmosphere for a midday, winter, midlatitude period of low solar activity with the 1976 U.S. Standard Atmosphere.

highest altitude at which c_o occurs on the actual sound speed profile as shown in Fig. 4-2. From Z_k to Z_f, the turnaround altitude, the sound speed is assumed to increase linearly from 295 m/sec to 590 m/sec. That is, sound speed is modeled by

$$c = c_o \qquad 0 \leqslant Z \leqslant Z_k \tag{4-1}$$

$$c = c_o\,[1 + \delta(Z - Z_k)] \qquad Z_k \leqslant Z \leqslant Z_f$$

$$\delta = \frac{(1 - \cos \theta o)}{\cos \theta_o (Z_f - Z_k)} \tag{4-2}$$

From Fig. 4-2 we see that the assumed profile is in good qualitative agreement with the actual profile. By using this simplified model, we reduce the ray paths to straight lines below Z_k and arcs of circles above Z_k. The actual sound speed profile above Z_k is not well known, and since our assumed straight line fits the best guess rather well, we will not concern ourselves with the

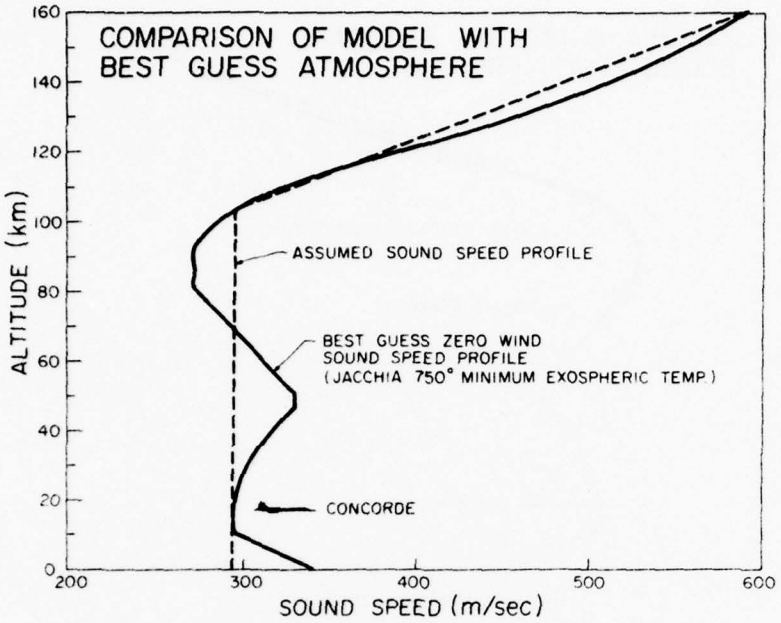

Fig. 4.2 – Comparison of sound speed for best guess atmosphere with the assumed sound speed profile

accuracy of our model atmosphere above $Z = Z_k$. To test the validity of our model below $Z = Z_k$ we performed the ray tracing for the U.S. Standard Atmosphere, for several initial angles. The results are shown in Figs. 4-3 and 4-4. For $\theta_o = 60°$, which corresponds to the on-axis case for a Mach number of 2, we see that our assumed straight line ray differs insignificantly from the actual ray. This is also the case for $\theta_o = 50°$. For $\theta_o = 40°$ the length of the two rays is nearly the same so the computed age and hence the final amplitude and frequency will be nearly the same. This is especially true since the vast majority of the aging occurs above Z_k. We will, however, in this case underestimate the propagation range by 10 km. For $\theta_o = 30°$ we would probably have some difference in the age and a significant error (60 km) in the propagation distance. An enormous error occurs when θ_o is less than 26° since in this case the wave never reaches the thermosphere but is reflected from below 50 km. Such a ray, however, would not reach the ground. Thus, with the U.S. Standard Atmosphere, *little* error, except for range predictions for $\theta \leqslant 40°$, is incurred by using an isovelocity profile below

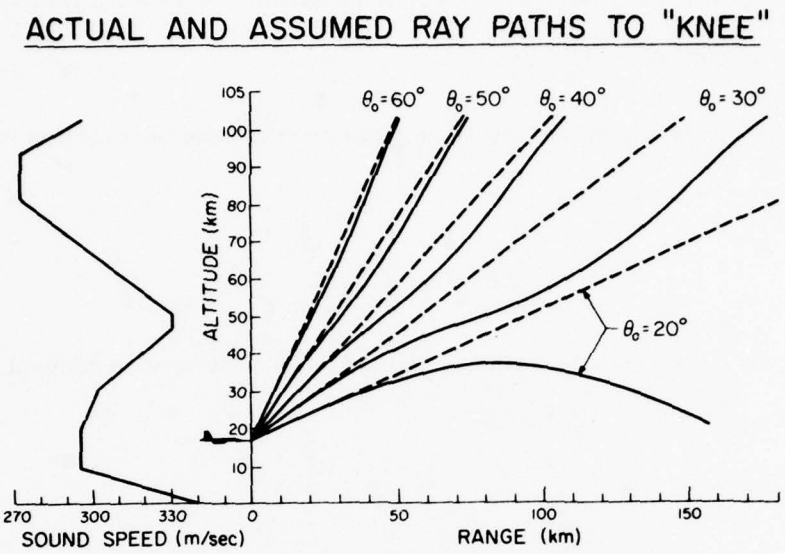

Fig. 4.3 — Comparison of ray paths to the thermosphere using our model (dashed lines) and best guess atmosphere (solid lines). Best guess sound speed profile shown on left of figure.

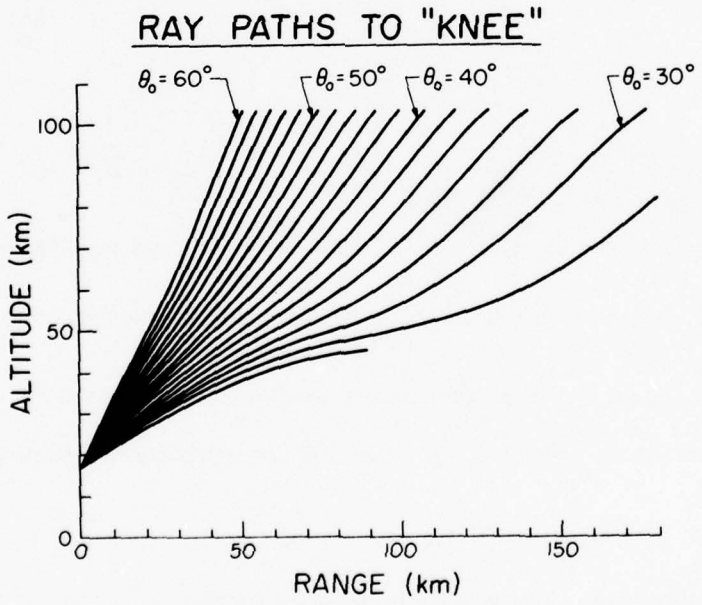

Fig. 4.4 — Ray paths to the thermosphere using best guess atmosphere sound profile.

Z_k. When winds blowing in the direction of the aircraft flight are present in the ozonosphere, for cases far enough off track, we may predict thermospheric returns when the return may actually be coming from below 60 km.

The pressure and density for our model are found by integrating the equations for hydrostatic balance.

$$\frac{dp}{dZ} = -\rho g = -\frac{\gamma p}{c^2} g \tag{4-2}$$

Again we break the integral into two regions, one where the sound speed is constant, and the other where $c = c_o[1 + \delta (Z - Z_k)]$. Then,

$$p/p_o = e^{-\left|\frac{Z - Z_o}{H_1}\right|} \qquad \text{for } Z < Z_k$$

$$p/p_k = e^{-\frac{Z - Z_k}{H_2[1 + \delta(Z - Z_k)]}} \qquad \text{for } Z_k < Z < Z_f \qquad p_k = p_o e^{-\left|\frac{Z_k - Z_o}{H_1}\right|} \tag{4-3}$$

where H_1 and H_2 are scale heights. The density is found from the relation $\rho = \frac{\gamma p}{c^2}$. Thus,

$$\rho = \rho_o e^{-\left|\frac{Z - Z_o}{H_1}\right|} \qquad Z < Z_k \tag{4-4}$$

$$\rho = \rho_k \frac{e^{-\frac{Z - Z_k}{H_2[1 + \delta(Z - Z_k)]}}}{[1 + \delta(Z - Z_k)]^2} \qquad Z_k < Z < Z_f \qquad \rho_k = \rho_o e^{-\left|\frac{Z_k - Z_o}{H_1}\right|}$$

Since the scale height is not constant with altitude, using the scale height computed from $H_s^{-1} = \frac{\gamma g}{c_o^2}$ will lead to an error in p and ρ at the final altitude. To overcome this we compute two scale heights H_1 and H_2 which are computed by matching the pressures at the turning point Z_k and the final altitude Z_f. This has the same effect as redefining an effective g for each region.

In the case with constant winds we have from Snell's law that

$$(c' + u) \cos \theta = c = c_o[1 + \delta(Z - Z_k)] \tag{4-5}$$

Solving for the top of the ray, where $\cos \theta \approx 1$, we can find the sound speed lapse rate δ. Both the model atmospheric properties and the ray equation are now completely defined. From Snell's law

$$\cos \theta = \frac{c_o[1 + \delta (Z - Z_k)]}{(c' + u)} \tag{4-6}$$

With the wind equal to zero at the Concorde fight altitude, we have

$$c' = \frac{c_o}{\cos \theta_o}.$$

5. Linear Attenuation

Acoustic attenuation in air at infrasonic frequencies is negligible at sea level (< .01 db/km).[23] At high altitudes, however, the attenuation of infrasound can become quite large because the acoustic attenuation per wave length is a function of f/p.[24] Thus at 160 km, where $p/p_g = 3 \times 10^{-9}$, the attenuation per wavelength at 1 Hz is equivalent to the sea level attenuation per wavelength at 333 MHz. (The subscript g will refer to values at sea level.) There are four major sources of acoustic attenuation in air; viscosity, heat conduction and the rotational and vibrational relaxation of O_2 and N_2. In this section we consider each of these mechanisms and obtain an attenuation model for the upper atmosphere.

A. Vibrational Relaxation

Vibrational relaxation, which is the dominant attenuation mechanism at low frequencies at atmospheric pressure, is extremely sensitive to the presence of trace constituents in the air, mainly water vapor and CO_2. For example, the attenuation at 1 kHz at 10% relative humidity is twice that at 20% relative humidity while at 20 kHz this relation is reversed.[23] We shall show, however, that for the effective frequencies (f/p) of interest, these complex vibrational relaxation processes are frozen out.

Of primary concern is the vibrational relaxation of O_2 since the relaxation frequency of N_2 is orders of magnitude lower.[25] At high humidities the vibrational relaxation frequency may exceed 100 kHz. However, above 100 km the concentration of water vapor is much less than 1 ppm[22] so we are interested in the relaxation frequency for dry air which is known to be between 30 and 40 Hz/atm.[23,26] In the absence of water vapor the vibrational relaxation frequency is

strongly influenced by the presence of minute quantities of CO_2. For CO_2-free air the relaxation frequency is 6 Hz/atm. Though the mixing ratio of CO_2 at 20 km is 320 ppm[22], it is reasonable to expect it to be significantly lower above 100 km. Thus, we expect the relaxation frequency above 100 km to be 6 Hz/atm, though it could conceivably be as high as 30 Hz/atm (which corresponds to 300 ppm CO_2). The lowest frequencies that we will be concerned with are of the order of .01 Hz which corresponds to 30 kHz/atm at 100 km and 3 MHz/atm at 150 km. Since these frequencies are many orders of magnitude larger than the largest conceivable value for the relaxation frequency, we can safely conclude that vibrational relaxation can be neglected.

B. Classical Attenuation

Heat conduction and viscosity are the dominant attenuation mechanisms in the thermosphere at infrasonic frequency. Together they comprise what is referred to as classical attenuation. The classical attenuation coefficient for air is given by

$$\frac{\alpha_{cl}}{f^2} = \frac{8\pi^3}{3\rho c^3}\left[\eta + \frac{3}{4}\left[\frac{\gamma - 1}{C_p}\right]\kappa\right] \tag{5-1}$$

where η is the shear viscosity, C_p the constant pressure heat capacity and κ the thermal conductivity. Since $p = \rho c^2/\gamma$, we can rewrite Eq. (5-1) as

$$\frac{\alpha_{cl} p}{f^2} = \frac{8\pi^3}{3\gamma c}\left[\eta + \frac{3}{4}\left[\frac{\gamma - 1}{C_p}\right]\kappa\right] \tag{5-2}$$

Thus α_{cl} is directly proportional to the square of the frequency and inversely proportional to ambient pressure. Equation (5-2) is valid below the translational relaxation frequency, i.e. as long as the wavelength is greater than a mean free path. From the kinetic theory of gases, the thermal conductivity and viscosity are related by the Euchen relation.[27]

$$\kappa = \left[\frac{9\gamma - 5}{4\gamma}\right] C_p\eta = \frac{19}{14}\, C_p\eta \tag{5-3}$$

Thus from Eqs. (5-2) and (5-3)

$$\frac{\alpha_{cl} p}{f^2} = \left[\frac{394\ \pi^3}{35\ \gamma}\right] \frac{\eta}{c} \tag{5-4}$$

so that the classical attenuation depends solely on the ratio η/c. The temperature dependence of the viscosity is given by Southerland's formula

$$\eta = \frac{b_o T^{3/2}}{T + 110.4}$$

where $b_o = 1.458 \times 10^{-6}$ kg/(sec-meter-°K$^{1/2}$).[22] If η_g is the viscosity at sea level then at 160 km

$$\eta = 1.856\ \eta_g$$

while

$$c = 1.735\ c_g$$

so that

$$\frac{\eta}{c} = 1.07\ \frac{\eta_g}{c_g} \tag{5-5}$$

from which we conclude that $\alpha_{cl} p/f^2$ is, to a good approximation, independent of temperature and hence altitude. We shall therefore use measured values of $\alpha_{cl} p/f^2$ appropriate to 20°C.

C. Rotational Relaxation

The rotational relaxations in O_2, N_2 and air behave like a simple single relaxation process. For such a relaxation process the attenuation coefficient is given by

$$\alpha_{rot}\lambda = \frac{2(\alpha_{rot}\lambda)_{max}\left[\frac{f p_g}{f_{rot} p}\right]}{1 + \left[\frac{f p_g}{f_{rot} p}\right]^2} \tag{5-6}$$

where f_{rot} is the rotational relaxation frequency at one atmosphere and $(\alpha_{rot}\lambda)_{max}$ is the maximum value of $\alpha_{rot}\lambda$, which is attained when $f = f_{rot}$. When the effective frequency, $\frac{f p_g}{p}$, is less than f_{rot}, Eq. (5-6) becomes

$$\frac{\alpha_{rot} p}{f^2} = \frac{2(\alpha_{rot}\lambda)_{max} p_g}{f_{rot} c} \tag{5-7}$$

Comparing Eqs. (5-2) and (5-7), we see that α_{cl} and α_{rot} both have the same dependence on pressure and frequency.

The temperature dependence of the right hand side of Eq. (5-7) presents some difficulties. It is known[28] that the rotational relaxation frequency, f_{rot}, for N_2 is temperature dependent decreasing from over 300 MHz at 295°K to around 75 MHz at 773°K.[28] This, however, is partially offset by the increase of sound speed and the decrease of $(\alpha_{rot}\lambda)_{max}$ with increasing temperature. Since the contribution of α_{rot} to the total attenuation is relatively small, and the data at high temperatures is sparse, we elected to ignore the temperature dependence of α_{rot}. It can be shown that this will result in underestimating α by no more than 25% at 160 km and by considerably less at lower altitudes.

D. Empirical Value for α

With the vibrational relaxation of O_2 frozen out, the attenuation in air and N_2 are virtually identical. Since the air below 160 km is primarily N_2, we shall use a value for α appropriate to a nitrogen atmosphere. In Fig. 5-1, taken from Greenspan,[27] experimental and theoretical values for $\alpha\lambda$ for N_2 are plotted as a function of Reynolds number. The values for the Reynolds number appropriate to our problem at 160 km and 120 km are indicated by the arrows. It is evident that we are operating well within the region where $\alpha p/f^2$ is a constant. That is, we are well above the Reynolds number at which either rotational or translational relaxation occurs. (With regard to the latter, at 160 km the mean free path is 53 m while our pulse length is about 4 km.)

The values quoted in the literature for α/f^2 for N_2 at atmospheric pressure are all in reasonably good agreement with one another. Values of 1.79×10^{-11} Neper $\cdot$ sec^2/m (Sessler),[29]

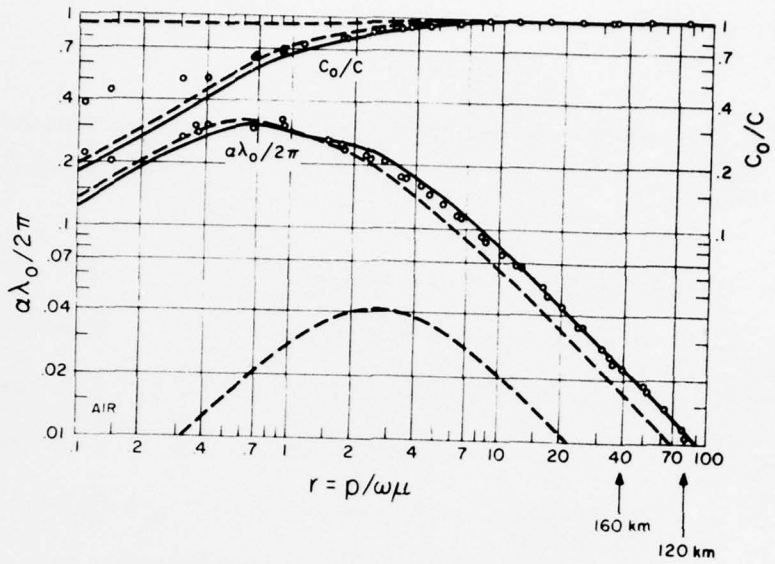

Fig. 5.1 — Attenuation per unit wavelength and sound speed for molecular nitrogen are shown as a function of Reynolds number. Reynolds numbers appropriate to the thermosphere for our problem are shown by the arrows. From Greenspan, J. Acoust. Soc. Am. **31**, 1950.

1.66×10^{-11} Neper · sec^2/m (Winter and Hill),[28] 1.64×10^{11} Neper · sec^2/m (Parker et. al.)[30] and 1.74×10^{-11} Neper · sec^2/m (Greenspan)[27] were averaged to obtain

$$\alpha = 1.70 \times 10^{-11} \left\{ \frac{p_g}{p} \right\} f^2 \quad \text{Neper/m} \tag{5-8}$$

with a standard deviation of .07. This is the value for the attenuation coefficient that we will use at all altitudes.

6. Linear Solution and Crossover Model

When the acoustic attenuation coefficient is proportional to f^2, as in Eq. (5-8), the Blokhintsev variable, in the absence of winds, satisfies the following reduced wave equation along a ray

$$\frac{\partial V}{\partial s} + \frac{\Gamma V}{c^2\sqrt{\rho c A_n}} \frac{\partial V}{\partial \tau} = a(s) \frac{\partial^2 V}{\partial \tau^2} \tag{6-1}$$

Here s is the distance along the ray, τ is the retarded time, and the attenuation factor $a(s)$ is defined by

$$a(s) = \frac{\alpha(s)}{\omega^2} \tag{6-2}$$

The attenuation factor depends on s due to the pressure dependence of α. Since the particle velocity is related to the Blokhintsev variable by

$$q = \frac{V}{\sqrt{\rho c A_n}} \tag{6-3}$$

Eq. (6-1) can be rewritten as

$$\frac{\partial V}{\partial s} + \frac{\Gamma q}{c^2} \frac{\partial V}{\partial \tau} = a(s) \frac{\partial^2 V}{\partial \tau^2} \tag{6-4}$$

For an N wave, where the time of the positive phase is given by t_p, the relative importance of the nonlinear term $\frac{\Gamma q}{c^2} \frac{\partial V}{\partial \tau}$ and the linear attenuation term $a(s) \frac{\partial^2 V}{\partial \tau^2}$ is measured by the ratio

$$R = \frac{\Gamma q t_p}{a c^2} \tag{6-5}$$

which is called the Gol'dberg number. When R is very large, the linear attenuation term can be neglected, yielding the inviscid Burgers' equation

$$\frac{\partial V}{\partial s} = \frac{\Gamma V}{c^2\sqrt{\rho c A_n}} \frac{\partial V}{\partial \tau} \tag{6-6}$$

which was solved in Section 3. When R is small, the nonlinear term can be neglected and the propagation is governed by the diffusion equation

$$\frac{\partial V}{\partial s} = a(s) \frac{\partial^2 V}{\partial \tau^2} \tag{6-7}$$

We assume that, at a given altitude, either Burgers' equation, Eq. (6-6), or the diffusion equation, Eq. (6-7), applies. This is possible because, due to the increasing α and c, the Gol'dberg number decreases rapidly with altitude so the region where the complete Eq. (6-4) is required is very narrow. An appropriate place to make the transition from Eq. (6-6) to Eq. (6-7) is where the incremental decrease in energy due to nonlinear attenuation becomes equal to the incremental decrease in energy due to linear attenuation. That is, we switch from Eq. (6-6) to Eq. (6-7) when

$$\frac{1}{E}\left(\frac{\partial E}{\partial s}\right)_{LINEAR} = \frac{1}{E}\left(\frac{\partial E}{\partial s}\right)_{NONLINEAR} \tag{6-8}$$

The energy in the N wave is proportional to $q_p^2 t_p$, where q_p is the peak value of the velocity and t_p is the time of the positive phase. From the N wave solution we obtain at any point s

$$\frac{1}{E}\left(\frac{\partial E}{\partial s}\right)_{NONLINEAR} = \frac{-\Gamma q_p}{2c^2 t_p} \tag{6-9}$$

The spectrum of the N wave has its maximum at $f_p \simeq \frac{1}{3t_p}$, so the linear energy attenuation coefficient is approximated by

$$\frac{1}{E}\left(\frac{\partial E}{\partial s}\right)_{LINEAR} = -2\alpha = -8\pi^2 a f_p^2 = -\frac{8\pi^2 a}{9t_p^2} \tag{6-10}$$

Equation (6-8) is thus satisfied when

$$R = \frac{\Gamma q_p t_p}{ac^2} = \frac{8\pi^2}{9} = 17.5. \tag{6-11}$$

We shall therefore use Eq. (6-6) when $R > 17.5$ and Eq. (6-7) when $R \leqslant 17.5$. [We note that Eq. (6-4) can be solved exactly when a is independent of s. We have examined the solution and found it consistent with this choice for the cross over value for R. At $R = 30$ the wave is definitely a weak shock and at $R = 10$ it is definitely linear.] We shall examine the consequences of modeling Eq. (6-4) in this way later on in greater detail.

Since the weak shock solution for an N wave is always an N wave, the initial condition for our solution to Eq. (6-7) will be an N wave. We assume that at the transition point s_L, the wave form is given by

$$V = -\frac{V_L \tau}{\tau_L} \qquad -\tau_L \leqslant \tau \leqslant \tau_L. \tag{6-12}$$

If we change variables from s to

$$\chi = \int_{s_L}^{s} a(s)\,ds \tag{6-13}$$

then Eq. (6-7) becomes

$$\frac{\partial V}{\partial \chi} = \frac{\partial^2 V}{\partial \tau^2} \tag{6-14}$$

which is a simple diffusion equation whose solution, subject to the given initial condition, is

$$\hat{V} = -\frac{1}{2}\,\hat{\tau}\left\{erf\left[\frac{\hat{\tau}+1}{2\xi_E}\right] - erf\left[\frac{\hat{\tau}-1}{2\xi_E}\right]\right\} - \frac{\xi_E}{\sqrt{\pi}}\left\{\exp\left[-\left[\frac{\hat{\tau}+1}{2\xi_E}\right]^2\right] - \exp\left[-\left[\frac{\hat{\tau}-1}{2\xi_E}\right]^2\right]\right\} \tag{6-15}$$

where $\hat{V} = V/V_L$, $\hat{\tau} = \tau/\tau_L$ and the "linear age" is defined by

$$\xi_E = \frac{\sqrt{\chi}}{\tau_L} \tag{6-16}$$

The waveform is plotted for several values of ξ_E in Fig. 6-1. For $\xi_E \gtrsim 1$, $\hat{V}$ approaches the form

$$\hat{V} = \frac{\hat{\tau}}{6\sqrt{\pi}\,\xi_E^{3}}\, e^{-\hat{\tau}^2/4\xi_E^2} \tag{6-17}$$

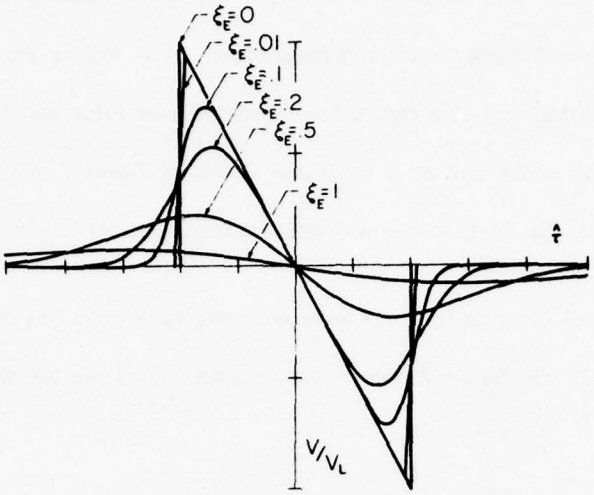

Fig. 6.1 — Waveform vs retarded time for several values of the age parameter showing effect of linear aging.

Equation (6-17) has a maximum at $\hat{\tau}_m = 2\xi_E$ so

$$\hat{V}_{peak} = \sqrt{\frac{2}{\pi e}} \frac{1}{6\xi_E^2} \qquad \xi_E \gtrsim 1 \tag{6-18}$$

Similarly, the energy is given by

$$\frac{E}{E_L} = \sqrt{\frac{2}{\pi}} \frac{1}{24\xi_E^2} \qquad \xi_E \gtrsim 1 \tag{6-19}$$

and the peak frequency by

$$\frac{f_{peak}}{f_L} = \frac{1}{\sqrt{2}\,\xi_E} \qquad \xi_E \gtrsim 1 \tag{6-20}$$

From these asymptotic forms and numerical analysis of Eq. (6-15), we can obtain simple empirical formulas for $\hat{V}_{peak}$, f_{peak} and E/E_L as a function of ξ_E

$$\hat{V}_{peak} = \frac{1 + .452e^{-14\xi_E}}{\left[1.452 - \frac{\xi_E}{5} + 6\sqrt{\frac{\pi e}{2}}\,\xi_E^2\right]} \tag{6-21}$$

$$\frac{E}{E_L} = \frac{1 - .17\xi_E e^{-5\xi_E}}{\left[1 + 2.5\xi_E + 1.3\xi_E^2 + 24\sqrt{\frac{\pi}{2}}\,\xi_E^3\right]} \tag{6-22}$$

$$f_{peak} = \frac{\epsilon}{\pi \tau_L} \left[\frac{1 + \frac{3.55}{\epsilon} \xi_E e^{-4\xi_E}}{\frac{1}{\epsilon} e^{-1.5\xi_E} + \sqrt{2}\, \xi_E} \right] \tag{6-23}$$

where $\epsilon = 2.0815760$ and $f_L = \frac{\epsilon}{\pi \tau_L}$. Equations (6-21)-(6-23), which are plotted in Fig. 6-2, are accurate to within 1% for all values of ξ_E. All of the pertinent information about the linear solution can easily be obtained from Eqs. (6-14), (6-20), (6-21), and (6-23) once one determines the linear age ξ_E. The problem is thus solved once one obtains χ from Eq. (6-13).

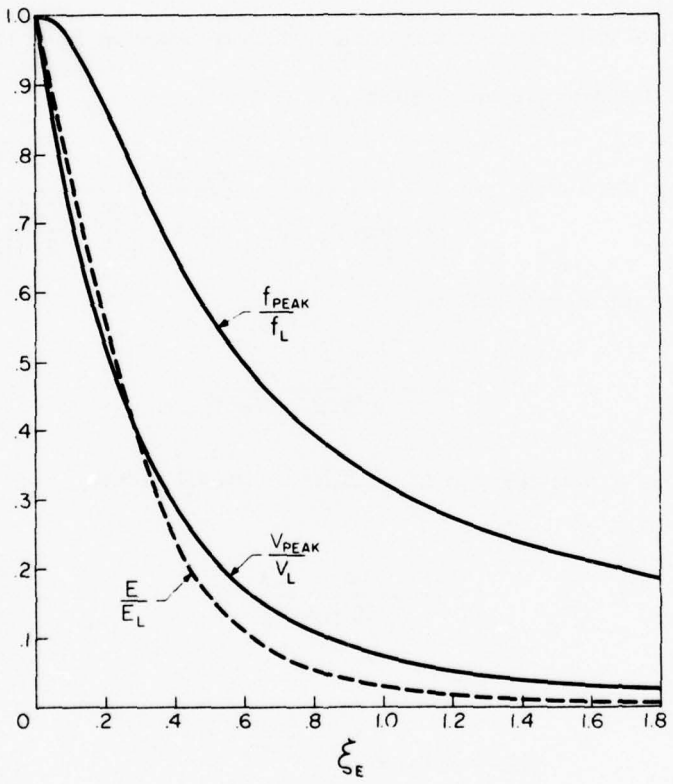

Fig. 6.2 — Decay of amplitude, peak frequency, and wave energy with increasing linear age.

The dependence of the attenuation factor on s is due solely to the dependence of the ambient pressure p on s. Hence

$$a(s) = \frac{a_g p_g}{p(s)} \tag{6-24}$$

where a_g and p_g are the attenuation coefficient and pressure at ground level.

In order to determine the value of the Blokhintsev variable V at the turning point, we evaluate χ_f, which is obtained from Eq. (6-13), by integrating $a(s)$ along the ray from the altitude Z_L (where $R = 17.5$) to Z_f (the turning point altitude). It turns out that Z_L will always be above the "knee" in the sound speed profile, which is located at $Z_k \simeq 103$ km. From our previous analysis, the static pressure is given by

$$p(Z) = p(Z_k) \exp\left[\frac{-(Z - Z_k)\cos\theta_o}{H_2\left[\cos\theta_o + (1 - \cos\theta_o)\left(\frac{Z - Z_k}{Z_f - Z_k}\right)\right]}\right] \tag{6-25}$$

where the scale height H_2 is defined by

$$H_2 = \frac{(Z_f - Z_k)}{\ln[p(Z_k)/p(Z_f)]} \tag{6-26}$$

The ray is an arc of a circle of radius $(Z_f - Z_k)/(1 - \cos\theta_o)$ so that

$$ds = \frac{(Z_f - Z_k)}{(1 - \cos\theta_o)}\, d\theta \tag{6-27}$$

and

$$p(\theta) = p(Z_k)\, e^{-\frac{(Z_f - Z_k)\cos\theta_o}{H_2(1 - \cos\theta_o)}\left[1 - \frac{\cos\theta_o}{\cos\theta}\right]} \tag{6-28}$$

The limits of integration are $\theta = 0$ and

$$\theta_L = \cos^{-1}\left[\cos\theta_o + (1 - \cos\theta_o)\left(\frac{Z_L - Z_k)}{Z_f - Z_k}\right)\right] \tag{6-29}$$

From Eqs. (6-13), (6-24), (6-27) and (6-28) we obtain

$$\chi_f = \frac{Z_f - Z_k}{1 - \cos\theta_o}\, \frac{a_g p_g}{p(Z_k)}\, e^B \int_{\theta_L}^{0} e^{\frac{B\cos\theta_o}{\cos\theta}}\, d\theta \tag{6-30}$$

where

$$B = \frac{(Z_f - Z_k)\cos\theta_o}{H_2(1 - \cos\theta_o)} \tag{6-31}$$

We now change variables from θ to $\zeta = \frac{1}{\cos\theta} - 1$ which gives

$$\chi_f = \frac{a_g p_g}{p(Z_k)} \frac{(Z_f - Z_k)}{[1 - \cos\theta_o]} e^{B(1-\cos\theta_o)} \int_0^{\frac{1}{\cos\theta_L} - 1} \frac{e^{-B\cos\theta_o \zeta}\, d\zeta}{(\zeta + 1)\,(\zeta + 2)^{1/2}\,\zeta^{1/2}} \tag{6-32}$$

From Eq. (6-28)

$$e^{B(1-\cos\theta_o)} = p(Z_k)/p(Z_f) \tag{6-33}$$

and since $a_g p_g / p(Z_f) = a(Z_f)$, Equation (6-32) becomes

$$\chi_f = \frac{a(Z_f)}{[1 - \cos\theta_o]} (Z_f - Z_k) \int_0^{\frac{1-\cos\theta_L}{\cos\theta_L}} \frac{e^{-B\cos\theta_o \zeta}}{(\zeta + 1)\,(\zeta + 2)^{1/2}\,\zeta^{1/2}}\, d\zeta \tag{6-34}$$

Since $B \cos\theta_o$ is a fairly large number, the most important contributions to the integral come from small values of ζ. We can thus make the substitution

$$(\zeta + 1)\,(2 + \zeta)^{1/2} = \sqrt{2}\left(1 + \frac{5}{4}\,\zeta\right) = \sqrt{2}\, e^{5\zeta/4} \tag{6-35}$$

and obtain

$$\chi_f = \frac{a(Z_f)\,(Z_f - Z_k)}{[1 - \cos\theta_o]\,\sqrt{2}} \int_0^{\frac{1-\cos\theta_L}{\cos\theta_L}} \frac{e^{-\left(B\cos\theta_o + \frac{5}{4}\right)\zeta}}{\zeta^{1/2}}\, d\zeta \tag{6-36}$$

or

$$\chi_f = \frac{a(Z_f)\,(Z_f - Z_k)}{[1 - \cos\theta_o]} \quad \frac{\pi}{2\left(B\cos\theta_o + \frac{5}{4}\right)}\, erf\left[\sqrt{\frac{\left(B\cos\theta_o + \frac{5}{4}\right)(1 - \cos\theta_L)}{\cos\theta_L}}\right] \tag{6-37}$$

The Blokhintsev variable at $Z = Z_f$ is given by Eq. (6-15) with $\xi_E(Z_f) = \sqrt{\chi_f}/\tau_L$

Having obtained Eq. (6-37), we are now ready to reexamine our treatment of the transition from weak shock theory to linear theory. Due to the properties of the error function, χ_f

turns out to be nearly independent of θ_L. That is, unless θ_L is very nearly equal to zero, the error function is almost exactly equal to unity. Hence, in general,

$$\chi_f \simeq \frac{a(Z_f)\ (Z_f - Z_h)}{(1 - \cos\theta_o)} \sqrt{\frac{\pi}{2\left|B\cos\theta_o + \frac{5}{4}\right|}} \tag{6-38}$$

The saturation effect comes about because, due to the nature of the ray path, the wave spends most of its time at the higher altitudes where the attenuation is most severe. Thus, most of the "linear aging" occurs near the top of the path and hence, it is relatively unimportant exactly where the wave started. As a result of this saturation effect, χ_f will generally be the same, independent of what we choose for the crossover value for the Gol'dberg number. From Eq. (6-18) the peak value of the Blokhintsev variable at the turning point is given by

$$\hat{V}_{\text{peak}}(Z_f) = \sqrt{\frac{2}{\pi e}}\ \frac{\hat{V}(Z_L)}{6\left|\xi_E(Z_f)\right|^2} \tag{6-39}$$

or, with χ_f constant,

$$\hat{V}_{\text{peak}}(Z_f) = \text{Const.} \times \left|t_p(Z_L)\right|^2\ \hat{V}(Z_L) \tag{6-40}$$

Since the propagation up to Z_L is governed by weak shock theory, the impulse, given by $t_p(Z_L)\ V(Z_L)$, is a constant independent of Z_L. Hence,

$$\hat{V}_{\text{peak}}(Z_f) = \text{Const.} \times t_p(Z_L) \tag{6-41}$$

Due to the nonlinear stretching of the pulse, t_p will increase with increasing Z_L. Thus, using a smaller value for the crossover Gol'dberg number would result in a larger value for $\hat{V}_{\text{peak}}(Z_f)$. However, as the wave propagates, small changes in altitude produce large changes in the Gol'dberg number but only relatively small changes in t_p. Hence, the exact value we choose for the crossover Gol'dberg number is not crucial. Doubling or halving the crossover Gol'dberg number changes our result by less than 2 dB.

The preceding results help illustrate an important point. Weak shock waves propagate much better in the upper atmosphere than acoustic waves of the same frequency. This is fairly evident from the fact that the energy of a weak shock wave attenuates asymptotically like $s^{-1/2}$ while the energy of a linear N wave attenuates like $s^{-3/2}$. Once linear attenuation takes over, the wave attenuates much more rapidly than it would have had the wave remained shocked. It is therefore reasonable to expect that once the wave becomes linear, it will never reshock. We therefore assume that once the wave becomes linear, it remains linear. Moreover, if we use weak shock theory to solve the entire problem, we will obtain an upper bound for the solution.

To evaluate $\hat{V}$ at some height Z other than Z_f, we replace the upper limit in Eq. (6-30) by the appropriate θ which is calculated by replacing Z_L by Z in Eq. (6-29). For the downgoing part of the ray, we replace θ as calculated above by $-\theta$. The integral is evaluated in the same manner as χ_f.

7. The Caustic

I. Introduction

The reflection of a wave by a continuously stratified medium produces a caustic. For the sonic boom the caustic coincides with the turning point for $\phi = 0$ and occurs somewhat beyond the turning point for $\phi \neq 0$. At the caustic the ray tube area $A_n = 0$, so the ray theory predicts an infinite pressure. The singularity, however, is integrable so the infinite value does not affect the calculation of either the nonlinear or linear age parameter. The linear problem can be solved exactly, at and in the vicinity of the caustic, in terms of Airy functions[31], but the nonlinear problem, to our knowledge, remains unsolved. One would expect that in the immediate vicinity of the caustic, the linear and nonlinear solutions would be quite different (e.g., the formation of a Mach stem, self refraction, etc.), so there would appear to be little advantage to using the Airy function solution in preference to the ray theory.

We shall, therefore, treat the caustic by combining the weak shock theory with the approach of Keller[32,33] and others[34,35,36]. Keller handles the caustic by assuming that when a wave passes through a caustic, the net effect is to introduce a $\pi/2$ phase shift to the waveform. We therefore compute the age by assuming that the amplitude is governed by ray theory (since the integral converges) and determine the waveform by introducing a $\pi/2$ phase shift at the caustic. Since the ray theory gives an infinite result at the caustic, we cannot use ray theory to determine whether or not the Mach number in the vicinity of the caustic becomes too large for weak shock theory to be valid. To determine whether the weak shock theory is still appropriate, we rely on the empirical observation that the focus factor, in practice, never exceeds five in

the case of a simple caustic[37,38]. If the Mach number is still sufficiently small when the focus factor equals five, we shall assume that the weak shock theory can be used through the caustic.

II. Analysis of "U" Wave

We model the caustic by assuming that the N wave undergoes a $\pi/2$ phase shift at the caustic and then continues aging. There is considerable empirical evidence that this, indeed, is what happens. In their study of focused booms, Wanner et al[37] show many sonic boom waveforms. In every case where a waveform can be identified with a ray which has passed through a caustic, the waveform has the U shape characteristic of an N wave with a $\pi/2$ phase shift.

To determine the effect of the caustic, we start with an N wave with amplitude V_c and period $2\tau_c$ as shown in Fig. (7-1)

$$V(\tau) = -\frac{V_c \tau}{\tau_c} \qquad -\tau_c \leqslant \tau \leqslant \tau_c \tag{7-1}$$

The Fourier integral of V is given by

$$V_\omega = -\frac{2V_c}{\tau_c}\left[\frac{\sin(\omega\tau_c)}{\omega^2} - \tau_c\frac{\cos(\omega\tau_c)}{\omega}\right] \tag{7-2}$$

After passing through the caustic, the waveform undergoes a $\pi/2$ phase shift and $V(\tau)$ becomes $U(\tau)$ given by

$$U(\tau) = \frac{1}{\pi}\int_0^\infty \cos(\omega\,\tau)\; V_\omega\, d\omega \tag{7-3}$$

$$U(\tau) = -\frac{2}{\pi}\; V_c\left[1 - \frac{\tau}{2\tau_c}\log\left|\frac{\tau+\tau_c}{\tau-\tau_c}\right|\right] \tag{7-4}$$

$U(\tau)$ and $V(\tau)$ are plotted in Fig. 7-1.

The function $U(\tau)$ has two real roots located at $\tau = \pm\tau_r$ with τ_r given by

$$\frac{\tau_r}{\tau_c} = .833556500 \tag{7-5}$$

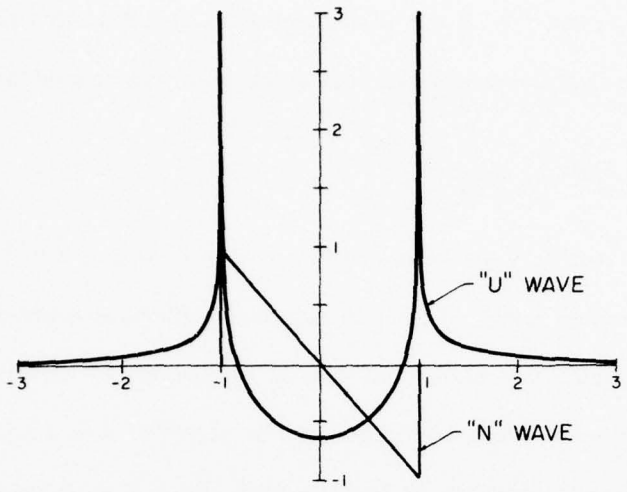

Fig. 7.1 — U wave results from a $\pi/2$ phase shift of the shown N wave

When the "U" wave ages into a "N" wave, the impulse from $\tau = -\infty$ to $\tau = -\tau_r$ will be contained in the first positive part of the N wave. Let $W(\tau)$ be the indefinite integral of $U(\tau)$. Then

$$W(\tau) \equiv \int U(\tau)\, d\tau = -\frac{V_c \tau_c}{\pi}\left\{\frac{\tau}{\tau_c} - \frac{1}{2}\left[\left(\frac{\tau}{\tau_c}\right)^2 - 1\right]\log\left|\frac{1+\frac{\tau}{\tau_c}}{1-\frac{\tau}{\tau_c}}\right|\right\}. \tag{7-6}$$

The first positive impulse of the "U" wave, I_U, is given by

$$I_U = W(-\tau_r) - W(-\infty) = \frac{V_c \tau_c^2}{\pi \tau_r} = .3819\ V_c \tau_c \tag{7-7}$$

while the positive impulse for the original N wave is given by

$$I_N = \int_{-\tau_c}^{0} V(t)\, dt = \frac{V_c \tau_c}{2} \tag{7-7a}$$

so that

$$I_U = .76373914\ I_N \tag{7-7b}$$

A. Exact Solution

A solution to the inviscid Burgers' equation

$$\frac{\partial V}{\partial \xi} = V \frac{\partial V}{\partial \tau} \tag{7-8}$$

where ξ is the age and τ the retarded time is

$$V = V(\tau + \xi V) \tag{7-9}$$

For the U wave at $\xi = 0$, $V(\tau)$ is given by Eq. (7-1). A "U" wave is shown for $\xi = 0$ and $\xi = \xi_A$ at the top and bottom of Fig. 7-2. For $\xi = \xi_A$ the wave has distorted according to Eq. (7-9) and a shock has formed. (The waveform will continue to age and will eventually turn back into an N wave.) V_A is the peak amplitude and $V_A - V_B$ the shock amplitude when $\xi = \xi_A$. In the initial waveform, V_A occurred at $\tau = -\tau_A$ and V_B occurred at $\tau = -\tau_B$. In the aged waveform, V_A occurs at $\tau = -\tau_A - \xi_A V_A$.

The area in region I in the top of Fig. 7-2 is equal to the area in region I in the bottom of Fig. 7-2. The same is true for region II. From Eq. (7-6) then

$$A_I = W(-\tau_r) - W(-\tau_A) \tag{7-10}$$

$$A_{II} = W(-\tau_B) \tag{7-11}$$

While from Fig. 7-2, we can see that

$$A_{III} = \frac{1}{2}\left[V_A^2 - V_B^2\right] \xi_A \tag{7-12}$$

Landau's law of equal areas[18] requires that the shock be located so that

$$A_I + A_{II} + A_{III} = W(-\tau_r) = I_U \tag{7-13}$$

so

$$W(-\tau_B) - W(-\tau_A) = \frac{1}{2}\,\xi_A\left[V_B^2 - V_A^2\right] \tag{7-14}$$

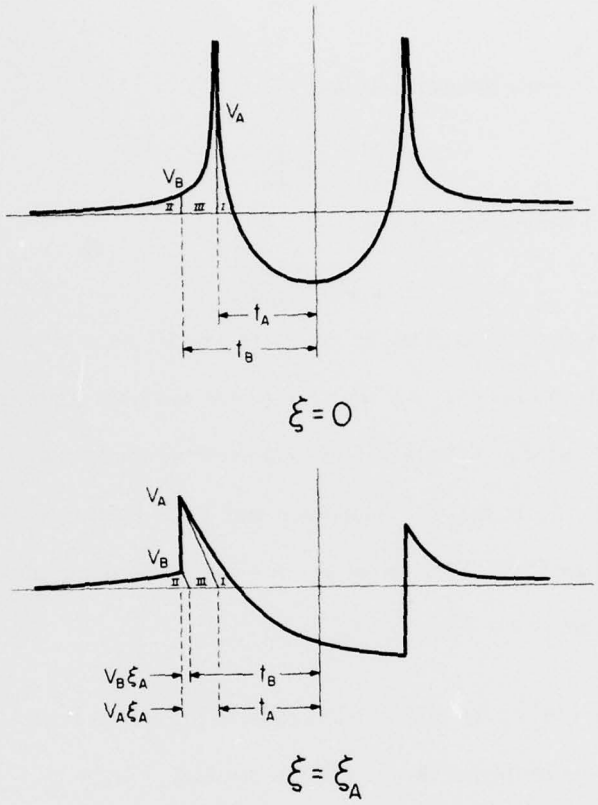

Fig. 7.2 — Nonlinear evolution of U wave towards the N wave final form.

By definition, when $\xi = \xi_A$ the retarded time for V_A equals the retarded time for V_B which is also the retarded time for the shock. Hence,

$$\tau_B + V_B\xi_B = \tau_A + V_A\xi_A \tag{7-15}$$

Equations (7-14) and (7-15) along with Eq. (7-6) for W and Eq. (7-4) for U can be solved numerically to give the peak value for U as a function of ξ. The result is shown in Table I. Note that the peak amplitude drops to reasonable values very quickly. For example, $U_{peak} = 4V_c$ by the time the age variable $\xi = .000015$ and is down to $2V_c$ when $\xi = .008$. This implies that we need not be concerned about the logarithmic singularity in the original U wave since it disappears very quickly. In any case the logarithmic singularity, which is due to

Table I

ξ	U_{peak}/V_c Exact	U_{peak}/V_c Eq. 7-20	U_{peak}/V_c Eq. 7-29
001.48×10^{-5}	4.0	1.38	1.07
000.0081	2.0	1.36	1.06
000.2231	1.0	1.11	0.883
001.705	0.5	0.60	0.517
009.814	0.25	0.27	0.2516
044.198	0.125	0.131	0.1253
186.35	0.0625	0.640	0.06254

the zero rise time of the N wave, would not actually be present for a real sonic boom which has finite rise time.

B. Reduction to an Equivalent "N" Wave

The peak value of the Blokhintsev variable V for an N wave is given by

$$V_{peak} = \sqrt{\frac{V_e \tau_e}{\frac{\tau_e}{V_e} + \xi}} \tag{7-16}$$

For an N wave whose initial amplitude was V_e and whose initial period was $2\tau_e$, the behavior of the wave is determined by two factors, the positive impulse $\frac{1}{2} V_e \tau_e$ (which is conserved) and the initial slope $-\frac{V_e}{\tau_e}$. It can be shown that, to a first approximation, the "U" wave goes over to an N wave whose impulse, $\frac{1}{2} V_e \tau_e$, equals the impulse of the first positive part of the "U" wave (I_U of Eq. 7-7) and for which $-\frac{V_e}{\tau_e}$ is equal to the slope of the "U" wave at $\tau = \tau_r$.

Now

$$\frac{\partial U}{\partial \tau} = \frac{V_c}{\pi \tau_c} \left[\log \left| \frac{\tau + \tau_c}{\tau - \tau_c} \right| - \frac{2\tau\tau_c}{\tau^2 - \tau_c^2} \right] \tag{7-17}$$

but since at $\tau = \tau_r$, $\log \left| \frac{\tau + \tau_c}{\tau - \tau_c} \right| = \frac{2\tau_c}{\tau_r}$, we have

$$\frac{V_e}{\tau_e} = \left.\frac{\partial U}{\partial \tau}\right|_{\tau=\tau_r} = \frac{2V_c\tau_c^2}{\pi\tau_r(\tau_c^2 - \tau_r^2)} = 2.5025574\ \frac{V_c}{\tau_c} \tag{7-18a}$$

while from Eq. (7-7b)

$$V_e\tau_e = .76373914\ V_c\tau_c \tag{7-18b}$$

Solving Eq. (7-18a) and Eq. (7-18b), we get

$$V_e = 1.38249812\ V_c \tag{7-19a}$$

$$\tau_e = .55243413\ \tau_c \tag{7-19b}$$

Hence, the equivalent N wave starts out with an amplitude about 1.38 times that of the original N wave and is about a little more than half as long. The equivalent N wave is shown in Fig. 7-3. To this approximation the peak amplitude is given by

$$U_{\text{peak}} = \sqrt{\frac{.7637\ V_c\tau_c}{.3996\frac{\tau_c}{V_c} + \xi}} \tag{7-20}$$

and the period of the positive phase by

$$t_p = .8739\ \sqrt{V_c\tau_c}\ \sqrt{.3996\ \tau_c/V_c + \xi} \tag{7-21}$$

Asymptotically

$$U_{\text{peak}} = .8739\sqrt{\frac{V_c\tau_c}{\xi}} \tag{7.22a}$$

$$t_p = .8739\sqrt{V_c\tau_c\xi} \tag{7.22b}$$

That is, both the amplitude and length are .8739 of what they would have been without the phase shift, i.e. had there been no caustic. U_{peak} from Eq. (7-20) is compared with the exact result in Table I.

C. Improved Analytical Model for "U" Wave

The disagreement between the exact result and the equivalent N wave result can be explained fairly easily. Consider the bottom of Fig. 7-2. The region to the right of the shock very quickly becomes half of an N wave as was assumed in deriving Eq. (7-20). The derivation, however, ignores the area to the left of the shock front. This area is not negligible until ξ

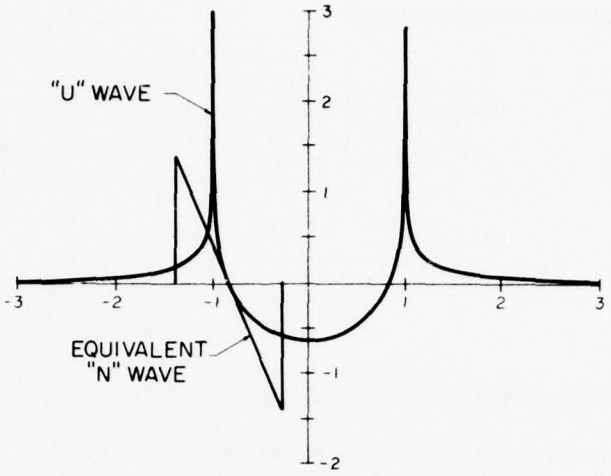

Fig. 7.3 — The asymptotic form of the equivalent N wave shown will be the same as the asymptotic form of the U wave for large age.

is quite large. Let A_L be the area to the left of the shock front and A_R be the area to the right of the shock front. The law of equal areas gives

$$A_R + A_L = I_U = (.7637)\ \frac{V_c \tau_c}{2} \tag{7-23}$$

If we assume that the waveform to the right of the shock is an N wave

$$A_R = \frac{1}{2}\ V_i^2 \left[\xi + .3996\ \frac{\tau_c}{V_c}\right] \tag{7-24}$$

We determine A_L by assuming that the relatively low amplitude waveform to the left of the shock is undistorted. The retarded time of the shock, τ_s, is given by

$$\tau_s = \left[-V_A \xi - .3996\ \frac{\tau_c}{V_c}\ V_A - \tau_r\right] \tag{7-25}$$

Since $U_B = U(\tau_s)$, and the waveform to the left of the shock is assumed to be undistorted, from Eq. (7-6)

$$A_L = -\ W(\tau_s) = -\ \frac{V_c \tau_c}{\pi}\left\{-\ \frac{\tau_s}{\tau_c} + \frac{1}{2}\left[\left(\frac{\tau_s}{\tau_c}\right)^2 - 1\right] \log\left|\frac{1 + \tau_s/\tau_c}{1 - \tau_s/\tau_c}\right|\right\} \tag{7-26}$$

For $\tau_s/\tau_c >> 1$ we can use the approximation

$$\log\left|\frac{1+\tau_s/\tau_c}{1-\tau_s/\tau_c}\right| \approx \frac{2\tau_c}{\tau_s} + \frac{2}{3}\left(\frac{\tau_c}{\tau_s}\right)^2 \tag{7-27}$$

so Eq. (7-26) becomes

$$A_L = \frac{2V_c\tau_c^2}{3\pi\tau_s} = \frac{2V_c\tau_c^2}{3\pi\left\{V_A\left[\xi + .3996\frac{\tau_c}{V_c}\right] + \tau_f\right\}} \tag{7-28}$$

Since A_L is a correction term, we let V_A in Eq. (7-28) be given by Eq. (7-20). Substituting the resulting expression in Eq. (7-28) and using Eqs. (7-23) and (7-24), we obtain for the peak value of the Blokhintsev variable

$$U_{\text{peak}} = \sqrt{\left[\frac{.7637\ V_c\tau_c - \frac{4}{3\pi}\left[\frac{V_c\tau_c}{\sqrt{.7637\frac{V_c}{\tau_c}(\xi + .3996) + .83356}}\right]}{\xi + .3996\frac{\tau_c}{V_c}}\right]} \tag{7-29}$$

Equation (7-29) is tabulated in Table I. It is seen to be a much better approximation when $\xi > 1$.

D. Solution for Linear Case

For the case where the Gol'dberg number has dropped below 17.5, the solution for V takes the form of Eq. (6-15) rather than an N wave. Since we are not especially interested in the exact value of V at Z_f, but rather the value at the ground, we shall use the same approach for the linear case as we did for the N wave. That is, we compute the linear age ξ_E right through the caustic, as we did in Section 6, and find the waveform by applying a $\pi/2$ phase shift to the waveform of Eq. (6-15). The phase shift does not affect the energy or spectral content of the wave so V_{peak} and $\frac{E}{E_L}$ are still given by Eqs. (6-21) and (6-22). Since ξ_E will

always be fairly large by the time the wave gets to the caustic, we compute the waveform by applying the $\pi/2$ phase shift to the asymptotic form for V given by Eq. (6-17). The result is

$$\hat{V}(\xi_E, \hat{\tau}) = -\frac{1}{3\pi\xi_E^2} + \frac{1}{6\pi}\frac{\hat{\tau}}{\xi_E^3}\sum_{k=0}^{\infty}\frac{(-1)^k k!}{(2k+1)!}\left[\frac{\hat{\tau}}{\xi_E}\right]^{2k+1} \tag{7-30}$$

The waveform before and after the caustic is shown for $\xi_E = 2$ on Fig. 7-4. The waveform has two small positive peaks and one large negative one given by

$$V_{\text{peak}} = -\frac{V_L}{3\pi\xi_E^2} \tag{7-31}$$

The peak pressure at the ground will thus be negative and 1.31 times larger than it would have been had there been no caustic.

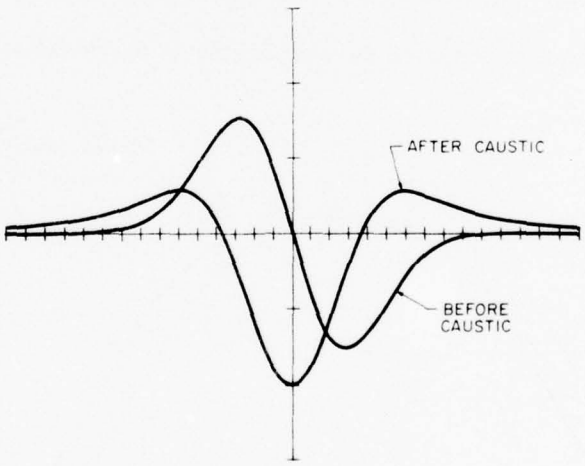

Fig. 7.4 — Typical linear wave form before and after $\pi/2$ phase shift at the caustic.

8. Results

The calculated ray paths for the initially upward and initially downward rays ($\phi = 0°$ and $\phi = 180°$, i.e. along flight path) are plotted in Fig. 8-1. As mentioned in Section 4, the rays are straight lines below $Z = Z_k$ and arcs of circles [in the case for $M = 2$, they have a radius of $2(Z_f - Z_k)$] between $Z = Z_k$ and the turning point at $Z = Z_f$. The formulas for computing the range for the various segments are shown on the figure. The initially upward ray travels a total horizontal distance of 310 km. The initially downward ray travels about 20 km farther. The upward traveling wave arrives at the ground in 22 minutes, which is 13 minutes after the Concorde has passed overhead (assuming it maintains its cruise velocity). That is, the average horizontal speed of the sonic boom is only about 2/5 that of the aircraft at cruise conditions.

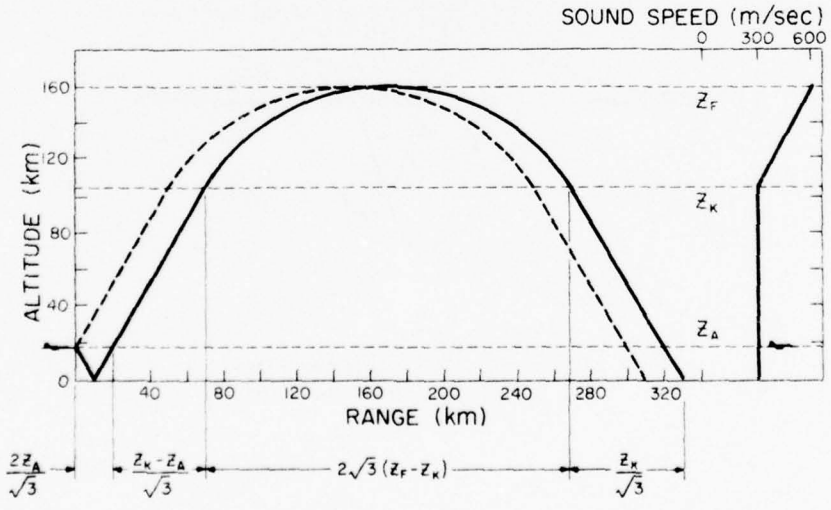

Fig. 8.1 — Upward and downward ray paths along ground track for Concorde flying at $M = 2$ using our assumed sound speed profile which is shown on the right of the figure. Formulas for computing ray distances at $M = 2$ are shown at bottom of the figure.

The initial conditions for N wave signature are found using the formulas of Carlson.[39] The formulas derived assume that the asymptotic form of the wave has been reached and the signature can be characterized by the bow shock overpressure and the signature duration. These can be computed in terms of a shape factor (which depends on the aircraft design), the distance from the aircraft, and the length of the aircraft.

$$\left(\frac{\Delta p}{p}\right) = K_p \sqrt{\frac{P_a}{p}} (M^2 - 1)^{1/8} \left(\frac{l_a}{h_c}\right)^{3/4} K_s$$

$$\Delta t = K_t \frac{3.42}{c_A} \frac{M}{(M^2 - 1)^{3/8}} \left(\frac{h_c}{l_A}\right)^{1/4} l_A K_s$$

Subscript A refers to values at the aircraft altitude. Values of K_s, K_t, and K_p are taken from charts in Reference 39. The value of K_s is a function of the lift parameter which in turn is a function of the azimuthal angle (proportional to -cos ϕ). Thus, the lift parameter is negative above the aircraft. Carlson, however, does not compute the shape factor for negative lift parameters. For the Concorde, at cruise conditions, the shape factor, determined by an extrapolation of Carlson's figure to negative lift parameters, would have a negative value. Since we do not know what the shape factor is for negative lift parameters, we have assumed a zero value above the aircraft, thus neglecting the negative lift contribution to the sonic boom in the upward direction. This will result in an overestimate of the strength of the upward boom. In the downward direction we can accurately obtain the shape factor as a function of azimuthal angle. We approximate Carlson's figure by $K_s = K_D(.4 - .6 \cos \phi)$ to obtain values off the flight track.

In order to treat the boom that initially starts downward and is then reflected from the ocean, we first calculate the boom overpressure and duration at sea level using Carlson's formulas. In order to compute the cylindrical ray tube spreading, we start the problem from sea level assuming that the aircraft is at the mirror image point below sea level. The calculation is then carried upward to the top and then back down again. For calculations of the upward

boom, we pick a point 4 km above the aircraft to start the problem. For the off track calculations, we use the correction formulas of Carlson to get the initial signal strength.

The results for $\phi = 0°$, and $\phi = 180°$, for the initial conditions discussed above, are given in Figs. 8-2, 8-3, 8-4,and 8-5 for the initially upward wave and in Figs. 8-6, 8-7 and 8-8 for the initially downward wave. Figure 8-2 shows $\Delta p/p$ as a function of altitude for the initially upward going wave. For comparison, the results of a modified "Garwin's Model", discussed in Section 2, are also shown. For this comparison the Blokhintsev invariant was held fixed, while the sound speed, density, and ray tube area were varied in the same manner as for the actual calculations. The results for both the nonlinear-linear (L) and nonlinear only (NL) solutions are orders of magnitude smaller than Garwin's model predicts. The nonlinear only solution predicts a maximum value of $\Delta p/p$ of .1, which corresponds to a Mach number of .07. The sharp rise in $\Delta p/p$ for both L and NL near 160 km is due to the influence of the caustic. From Fig. 8-2 it is evident that once the linear attenuation takes over, the Mach number decreases rather quickly. In Fig. 8-3 the Gol'dberg number is plotted as a function of altitude. The Gol'dberg number decreases rapidly with altitude in the vicinity of the crossover, as required by our model. Note that the Gol'dberg number decreases much more rapidly after the transition value when linear attenuation is included, thus justifying our "once linear always linear" hypothesis which we use in calculating the pressure on the ground for cases where linear attenuation becomes important. In Figure 8-4 the ratio of the remaining energy to the initial energy is plotted as a function of altitude. The energy decreases rapidly with height even when linear attenuation is not included. When linear attenuation takes over, however, the decrease in energy is much more marked. Note that the wave has lost 90% of its energy by the time it reaches 100 km and 99% of its energy by the time it reaches 140 km. Figure 8-5 shows the fundamental frequency $\left\{\frac{1}{2t_p}\right\}$ which is seen to decrease monotonically with altitude. The peak frequency, f_{peak}, is 2/3 of the value shown.

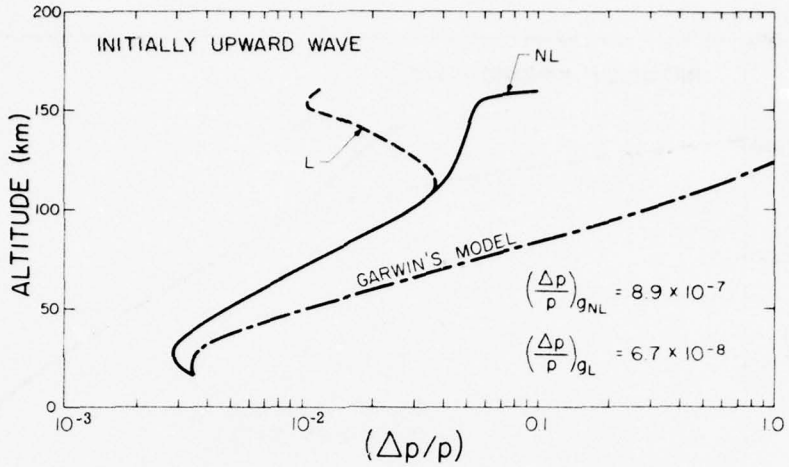

Fig. 8.2 — Relative signal strength as a function of altitude for an intially upward going ray along the ground track. Nonlinear only (NL) shown by solid line. Result with linear attentuation included (L) shown by broken lines. For comparison, the result of Garwin's model is shown (no attenuation included).

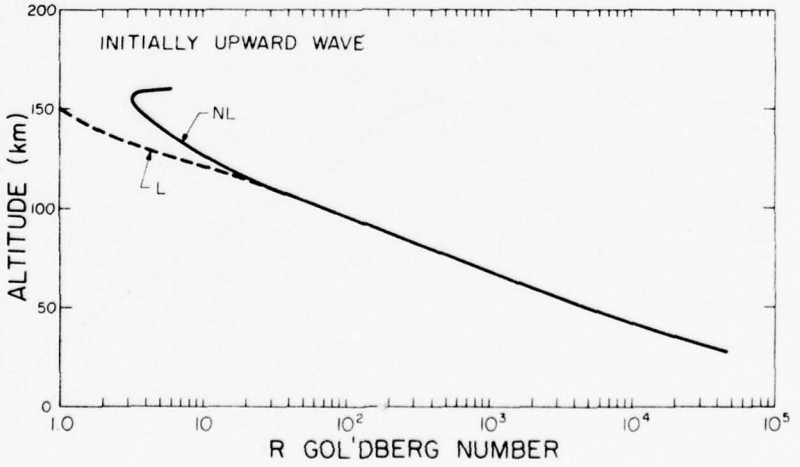

Fig. 8.3 — Gol'dberg number as a fuction of altitude. This number is a measure of relative importance of nonlinear and linear effects. Solid curve (NL) is from calculation based only on the nonlinear results.

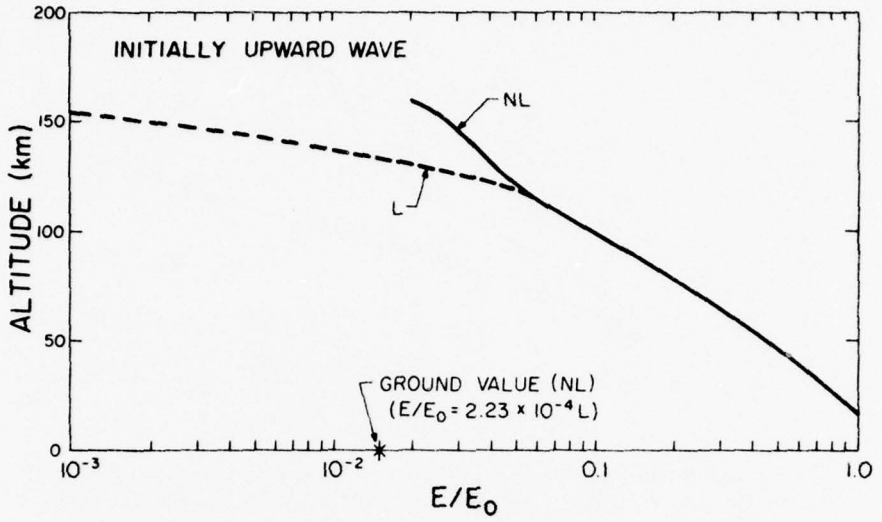

Fig. 8.4 — Ratio of energy in initially upward wave to initial energy as a function of altitude. Again NL and L refer to results which exclude and include linear attenuation respectively.

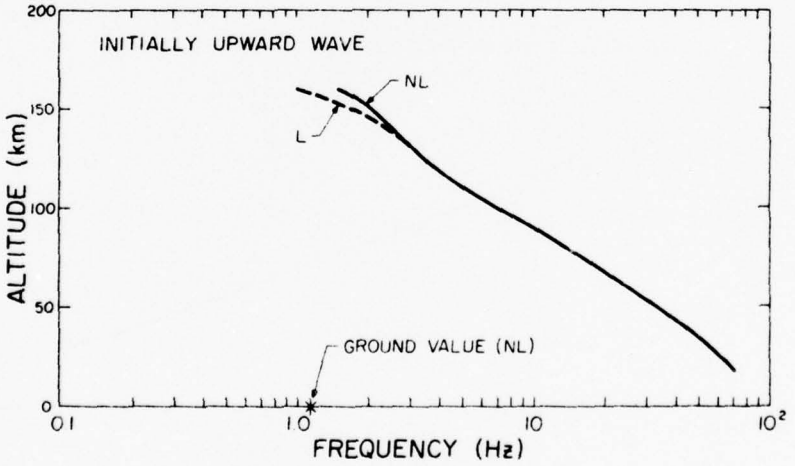

Fig. 8.5 — Fundamental frequency of initially upward wave ($2/3\, f_{peak}$) as a function of altitude.

Figures 8-6 to 8-8 show $\Delta p/p$, E/E_o and fundamental frequency vs altitude for the initially downward wave. The initially downward wave is the stronger of the two and is thus the most likely signal to be observed at the ground. This is compounded by the fact that, due to the uncertainty in the lift factor, we have probably overestimated the initially upward boom. Due to the higher initial amplitude and longer length of the initially downward wave, the transition to linear attenuation occurs at a higher altitude and hence linear attenuation is a less important factor. Most of the previous observations about the initially upward wave hold for the initially downward wave. Ninety percent of the energy is absorbed below 100 km, the Mach number never exceeds .1, and the frequency decreases monotonically with altitude.

Figure 8-9 shows the ground pressure for the initially upward and initially downward waves as a function of distance from the ground track. The solid lines show the combined linear-nonlinear results, the dashed lines the result obtained using nonlinear theory alone. The latter can be considered to be an upper bound for the ground pressure. The dominant signal is from the initially downward wave. The highest pressure level (about .3 Pa) will occur about 300 km from the ground track. The pressure measured on the ground track is a minimum and will be about .1 Pa for the initially downward wave. This is in contrast to the carpet boom, where the pressure is a maximum along the ground track. The sharp cutoffs, indicated by the vertical dashed lines at 380 and 425 km, are due to the fact that for values of $1/\cos\theta_o < 1.13$, the waves will be refracted upwards by the sound speed gradient in the lower troposphere before reaching the ground.

The only available quantitative data directly applicable to the problem of Concorde sonic boom returns from the thermosphere has been taken by Lamont-Doherty Geological Observatory.[5] They have been monitoring Concorde sonic booms on a regular basis using a tripartite array of microbarographs separated by about 1 km. They record amplitudes of the pressure signal with either a .1 to 1 Hz or 1 to 10 Hz bandpass. We compare our shock strength and signal

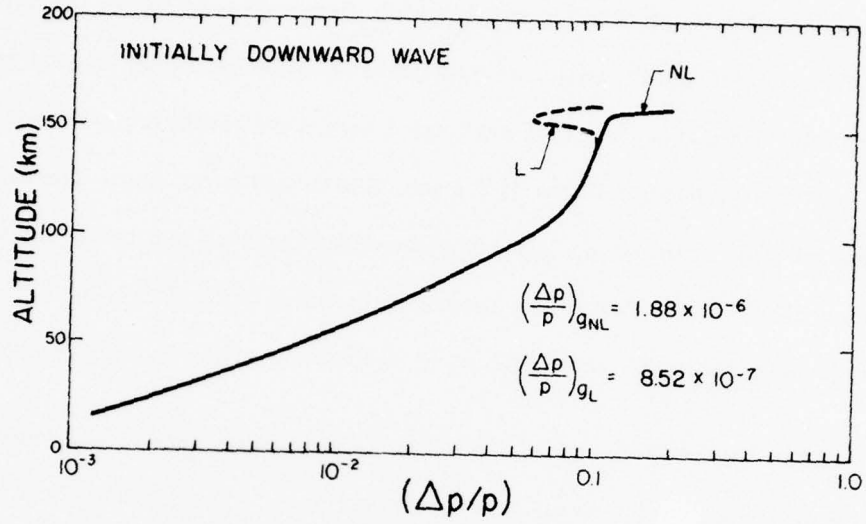

Fig. 8.6 — Relative signal strength as a function of altitude for an initially downward wave along the ground track.

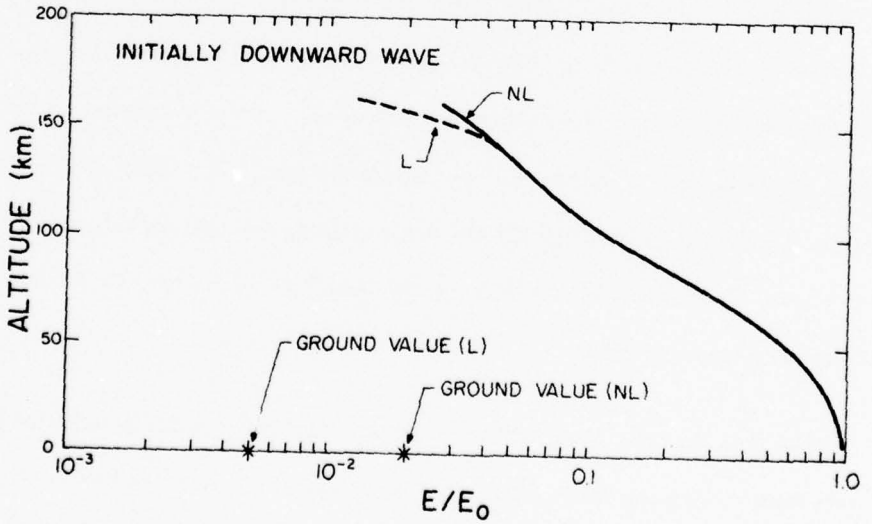

Fig. 8.7 — Ratio of energy in initially downward wave to initial energy as a function of altitude. Note that 90% of the energy is gone by 100 km and 99% gone by turnover point.

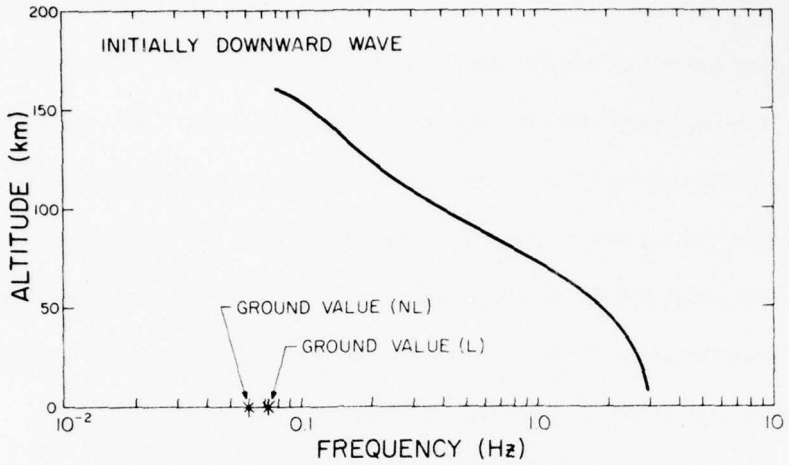

Fig. 8.8 — Fundamental frequency of initially downward wave ($2/3\ f_{peak}$) as a function of altitude.

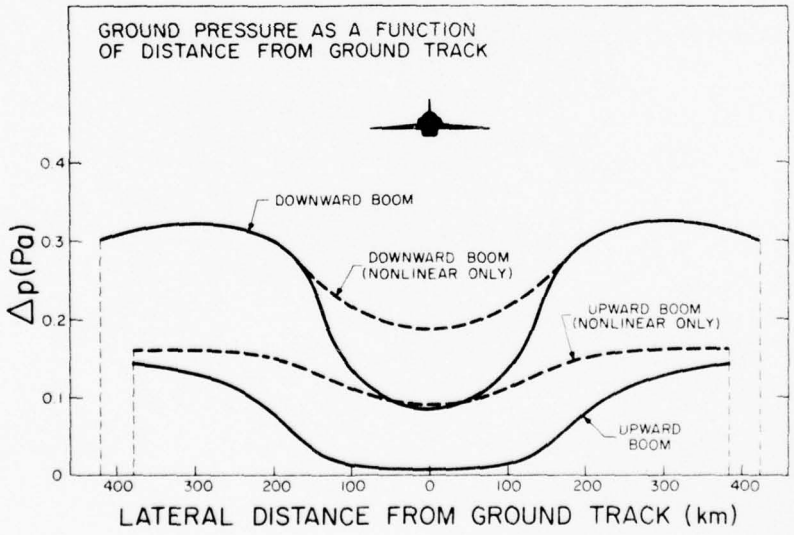

Fig. 8.9 — Relative signal strength on the ground from a sonic boom returning from the thermosphere as a function of lateral distance. Cutoff is determined by returning rays which are refracted upward before reaching the ground.

period with their peak amplitude and frequency. Lamont reports peak pressure of .1-.5 Pa and periods in excess of 8 seconds for signals identified as those returning from the thermosphere at an altitude of approximately 125 km. We predict an amplitude of .3 Pa and a period of 8.5 seconds for a wave returning from 125 km. Analysis of the ray tracing indicates that the origin of this wave is in disagreement with the analysis given in their report. We predict the origin to be further away and at bearing 11° from the one stated. We believe the origin of the difference lies in the difficulty of accurately determining bearing at such low frequencies with a 1 km array. Lamont lies about 230 km off the ground track we believe the Concorde to be on while generating the signal received. From Figure 8-9 we see for this distance off track, the received signal would be as large as will be measured anywhere.

Our results are also in qualitative agreement with the measurements done at Blacknest.[40] The period of the positive phase of explosion waves which return from the thermosphere are also in qualitative agreement with the results shown here, which indicates that our theory reasonably describes shock waves which propagate to the thermosphere and return.[41]

9. Strong Shock, Gravity, Turbulence and MHD Effects

In this section we discuss a number of physical effects which have not been included in our model. Our objective is to demonstrate that these effects will either have no effect on the solution or result in our model over estimating the ground pressure levels.

A. Strong Shock Effects

The intensification of upward propagating shock waves due to the decreasing density is a well known phenomenon.[42] It does not, however, appear to be an important consideration for the Concorde problem. Although our model does predict substantial increases in the Mach number, the process seems to be self-limiting. In no case does the Mach number greatly exceed 0.1 which is a conservative limit for the validity of weak-shock theory.[43,44] This is most likely due to the fact that the wave spends proportionately more time in regions of lower density and the resulting augmentation of the aging process decreases the Mach number almost as fast as the decrease in density increases it. The smallness of the Mach number assures both the validity of the weak shock theory and that the wave will not produce any serious perturbations of the atmosphere.

B. Gravity Effects

When an element of fluid is displaced upward or downward from its equilibrium position, the gravitational or buoyancy force will act to return the element to its equilibrium altitude. A fluid element thus displaced will tend to oscillate harmonically with an angular frequency given by

$$\omega_b \approx \sqrt{\frac{g}{\rho}\frac{\partial \rho}{\partial Z}} = \sqrt{\frac{g}{H_S}} \qquad (9\text{-}1)$$

This frequency is known as the Brunt-Vaisala frequency.[45] The effect of this additional restoring force is to introduce dispersion and anisotropy to the sound speed as well as the possibility of a resonance in the vicinity of the Brunt-Vaisala frequency. None of these effects will be important as long as the frequencies of interest are large in comparison with the Brunt-Vaisala frequency or, equivalently, as long as the wavelength is much less than the scale height.

The gravitational field will have its most pronounced effect for vertical propagation. For this case the phase velocity is given by[46]

$$v = c\sqrt{1 + \frac{1}{8\pi}\left[\frac{\lambda}{H_s}\right]^2} \qquad (9\text{-}2)$$

At 160 km, H_s = 26 km while λ = 4.8 km. Hence v/c = 1.0007. At 17 km, H_s = 6.9 km while λ = .03 km. Hence, v/c = 1.0000004. The amplitude effects will be of a similar size. We conclude that gravitational effects are of no consequence.

Turbulent Effects

In the above discussions we have assumed that the atmosphere was steady and stratified horizontally. The real atmosphere is known to be unsteady and turbulent. The scale of the inhomogeneities ranges from large scale weather phenomena such as fronts and storm systems, to internal waves, to turbulent fluctuations which may have a scale length down to fractions of an inch. Most of the work that has been done on the effect of turbulent fluctuations on sonic booms has looked at the effect in the region below 3000 ft, in the earth's turbulent boundary layer.[38,47] The primary effects that can be noticed on the boom signature consist of random fluctuations in signal strength behind the shock and an increase by several orders of magnitude in the thickness of the shock front.

Pierce and Maglieri[38] have shown that atmospheric turbulence can cause variations in waveform (from rounded to spiked with corresponding peak amplitude variations of ± 8 dB).

These variations occur both in time (i.e. as measured at one point from two identical aircraft passing overhead at a 5 sec interval) and in space (i.e. as measured by several microphones along the flight path of a single aircraft). This variability makes the problem difficult to characterize. Work by Crow,[48] George,[49] Cole and Friedman,[50] have attempted to explain the anomalous rise times and pressure flucuations in terms of scattering theories. Pierce attempts to explain the results in terms of a wave front folding mechanism.[47] George and Plotkin[51] developed a theory where the nonlinear steepening just balances the scattering to determine the anomalous rise time of the shocks. All of these mechanisms tend to enhance the dissipation of the wave or leave it unchanged. There are three reasons for this:

1. Pierce and Maglieri[38] have shown that the spectra of the spiked and rounded waveforms are virtually identical for frequencies up to about twice f_{peak}. Since long range propagation is determined primarily by the lower frequencies, one would expect distant arrivals of both waveforms to be nearly the same.

2. The Gol'dberg number for the spike of the spiked waveform will be much lower than for the wave as a whole because its duration is much shorter. One would therefore expect that in the thermosphere, where the attenuation is high, the propagation of the spike would be dominated by linear attenuation and thus the spike would soon disappear.

3. Turbulence increases the effective acoustic attenuation. Thus the Gol'dberg number will be lower and linear attenuation will take over sooner.

Thus a theory that ignores the effects of turbulence on the signal will give an upper bound on the signal strength. More importantly, the highest levels of turbulence are near the ground where the paths we are considering spend very little time. Most of the attenuation occurs at the higher altitudes in the thermosphere where turbulence plays no role.

In addition to turbulence, which may alter the local signal shape, unsteady inhomogeneities in the atmosphere may be responsible for another effect which has been observed for signals returned from the stratosphere. That is, most of these signals, rather than having a single cycle corresponding to an N wave, seem to have several cycles which may correspond to several N waves. Returns from the thermosphere, however, seem to be relatively clean having only the single cycle.[5.41]. This multiple cycle result may be due to the multipathing of signals which are bent over along different paths, depending on the unsteady component of the ray velocity. This effect should be most pronounced near where the ray turns over. A slight change in wind or sound speed could result in the ray traveling a higher or lower path. The fact that this multiple signal seems to come primarily from the stratospheric and tropospheric regions, but not from the thermosphere, may be a good indication that the thermosphere is relatively steady. The thermospheric rays pass through the region of unsteady flow at such a steep angle that they are virtually unaffected by this variation. Multipathing may result in some enhanced signal if two paths happen to come together with their phases matched, but there will also be regions where the signal would be diminished. Increases in strength of the signal by more than a factor of two seems highly unlikely since it would require more than two paths to simultaneously arrive at a point in phase. The major effect of such multipathing seems to produce signals which are spread out in time and involve several cycles.

Another effect not included in the model is that due to steep wind and temperature shear layers which have a scale length of the same order as the boom wavelength. In these regions geometric acoustic theory is not valid. If such regions exist, they will produce both a reflected and a transmitted wave from the shear layer (unless the velocity becomes large enough to reflect the wave completely). If such shear layers are weak, they will have only a small effect on the results, but in any case, the result will be to reflect some part of the wave energy at a lower altitude. Thus our model will provide an upper bound on the energy which reaches the

thermosphere. Any energy which is reflected from a lower altitude will have the properties of a wave which would have been refracted at that altitude (i.e. will have a shorter pulse duration than a wave refracted from a higher altitude). Since this mechanism will tend to split up the energy in the wave, its primary effect should be to weaken the wave. We are not aware of any evidence which suggests that any strong wave is reflected to the ground by this mechanism.

Plasma effects

Since the atmosphere at 160 km is partially ionized, the possibility of exciting MHD waves which may propagate at a faster rate than the neutral fluid wave exists. If we look at the collision frequency for scattering of charged particles by the neutral fluid, we have $\nu_a = n_f \sigma_{\alpha\alpha} \left(\frac{T_f}{m_\alpha} \right)^{1/2}$ $\sec^{-1}$, where n_f is the neutral density and $\sigma_{\alpha\alpha}$ is the cross section, approximately equal to 5×10^{-15} cm^2. A temperature of 10^3 °K and a molecular weight of about 20 give a collision frequency of about $\nu_a = 4.33$ $\sec^{-1}$ or about 4 collisions per second. The ratio of ion to neutral density is about 10^{-5} so that every one fourth second, 10^{-5} of the energy of the wave may be transferred to the ions. The wave spends no more than about 250 seconds in the region above 140 km (where the ion-neutral ratio is $>10^{-6}$). Thus about $4 \times 250 \times 10^{-5} = 10^{-2}$ of the neutral energy may be transferred to the ions as the wave passes through the thermosphere. Even if we assume that this energy does the most destructive thing possible, this is too small an amount of energy to seriously affect our results.

10. Summary and Conclusions

We have developed a model for the thermospheric propagation of the sonic boom from a Concorde aircraft. The model, which is for the most part analytic, accounts for all the physical effects which we believe to produce a significant effect on the result. From the results obtained with this model, we reach the following conclusions:

1. The $\Delta p/p$ in the thermosphere never exceeds .2. This implies that the weak-shock model is valid and that no large perturbations of the thermosphere (such as high temperatures which might produce strange lights) will occur.

2. Most of the energy in the wave is lost below 100 km. There is thus insufficient energy remaining in the wave to cause winds nearly as large as those which naturally occur in the thermosphere.

3. The wave will reach the ground at a horizontal distance of about 320 km from where it was launched.

4. For ray paths along the flight track, the Concorde will pass overhead approximately 13 minutes before the first arrival of the boom from the thermosphere (assuming that the Concorde continues at its cruise speed from the time the wave is launched). The average horizontal velocity of the sonic boom is less than half that of the Concorde at cruise conditions. It is thus highly unlikely that there could exist reasonable conditions of deceleration under which the boom would precede the aircraft.

5. The sound received along the ground track is a minimum. The largest signals will be observed from 200 to 400 km from the ground track.

6. The sound received will in all cases be small ($\lesssim$ .5 Pa) and of very low frequency ($\lesssim$ .1 Hz).

We conclude that thermospheric returns from Concorde are of sufficiently low amplitude and frequency that it is unlikely that they are either responsible for the East Coast events or likely to disturb the public. In addition we conclude that the sonic boom from the Concorde does not have sufficient amplitude or energy to produce a deleterious effect on the thermosphere.

Acknowledgments

The authors have benefited from consultations on various aspects of the problem with staff members from the National Oceanographic and Atmospheric Administration, the National Aeronautics and Space Administration, Sandia Laboratories, Lamont-Dougherty Geophysical Observatory, Bristol University, British Aerospace, ONR (London) and many colleagues at the Naval Research Laboratory. In particular we wish to thank Jack Reed of Sandia for providing data on long range propagation of explosive signals, and Andy Weiner of NRL for doing much of the numerical analysis in Chapter 6. We gratefully acknowledge many useful discussions and helpful suggestions from Drs. Tom Georges and Al Bedard of NOAA (Boulder), Bill Hass and Al Taylor, NOAA (Silver Spring), Domenic Maglieri and Harry Carlson, NASA (Langley), Tom Lawson and Bob Adams of Bristol University, Martin Lesson and Aubrey Price, ONR (London), Dick Thornborough and Doug Vickery, British Aerospace, A. R. George, Cornell University, William Donn, Lamont Geophysical Observatory, Lee Van Buren NRL/USRD (Orlando) and David Book, Elaine Oran, Mark Schoeberl, Darrell Strobel, and Ed Szuszczewicz of the Naval Research Laboratory. We would also like to thank Mr. Jack Brown for his continued guidance throughout this project.

REFERENCES

1. Science, **199**, 1416 (31 March 1978).

2. Physics Today, 61-63 (June 1978).

3. "NRL Investigations of East Coast Acoustic Events 2 December 1977-15 February 1978" (March 1978).

4. Garwin, R. L., "Speculation on Long-Range Effects of Supersonic Flight," unpublished (15 March, 1978).

5. Balachandian, N. K., Donn, W. L., and Rind, D. H., "Concorde Sonic Booms as an Atmospheric Probe," Science, **197**, No. 4298, 47-49 (July 1977).

6. Adams, R. D., Lawson, T. V. Aplin, P. S., "The Bumps In the Night," unpublished (1978).

7. *CIRA 1972, COSPAR International Reference Atmosphere 1972*, compiled by COSPAR Working Group 4, A. C. Stickland Ed. (Akademic-Verlang, Berlin, 1972).

8. Hayes, W. D., "Geometric Acoustics and Wave Theory," Second Conference on Sonic Boom Research, May 9-10, 1968, NASA SP-180, 159-164 (1968).

9. Hayes, W. D., Haefeli, R. C. Kulsrud, H. E., "Sonic Boom Propagation in a Stratified Atmosphere, with Computer Program," NASA CR-1299 (1969).

10. Blokhintsev, D. J., "The Propagation of Sound in an Inhomogeneous and Moving Medium, Part I," J. Acoust. Soc. Am. **18**, 322-334 (1946).

11. Garret, C. J. R. "Discussions: An Adiabatic Invariant for Wave Propagation in a Nonuniform Moving Medium," Proc. Roy. Soc. (London) Ser A, **288**, 26-27 (1967).

12. Hayes, W. D., "Energy Invariant for Geometric Acoustics in a Moving Medium," Phys. Fluids, **11**, 1654-1656 (1968).

13. Hayes, W. D., "Pseudotransonic Similitude and First-order Wave Structure," J. Aeron. Sci., **21**, 721-730 (1954).

14. Whitham, G. B., "On the Propagation of Weak Shock Waves," J. Fluid Mech. **1**, 290-318 (1956).

15. Whitham, G. B., "A New Approach to Problem of Shock Dynamics Part I, Two Dimensional Problems," J. Fluid Mech., **2**, 115-171 (1957).

16. Whitham, G. B., "A New Approach to Problems of Shock Dynamics Part II, Three Dimensional Problems," J. Fluid Mech., **5**, 369-386 (1959).

17. Crussard, L., "Sur la propagation et l'alteration des ondes de choc," C. R. Acad. Sci. Paris **156**, 611-613 (1913).

18. Landau, L. D. and Lifshitz, E. M., "Sound Waves in Second Approximation," Sec. 78 of *Mechanics of Continuous Media* (Gostekhizdat, 1944) or, "Formation of Discontinuities in a Sound Wave," Sec. 95 of *Fluid Mechanics* (Pergamon Press, 1959).

19. *Handbook of Mathematical Functions*, Abramowitz, M. and Stegun, I. A. Eds. (U. S. Government Printing Office, Washington, D. C., 1964) p. 298.

20. Op cit, p. 260.

21. Jacchia, L. G., J. Geophys. Res. **76**, 4602 (1971).

22. *U. S. Standard Atmosphere, 1976* (U. S. Government Printing Office, Washington, D. C., 1976).

23. Evans, L. B., Bass, H. C. and Southerland, L. C., J. Acoust. Soc. Am. **51**, 1565-1575 (1972).

24. Beyer, R. T. and Letcher, S. V., *Physical Ultrasonic* (Academic Press, N.Y. 1969) p. 109.

25. Piercy, J. E., J. Acoust. Soc. Am. **46**, 602-604 (1969).

26. Ref. 24, p. 113.

27. Greenspan, M. J., Acoust. Soc. Am. **31**, 155-160 (1959).

28. Winter, T. G. and Hill, G. L., J. Acoust. Soc. Am. **42**, 848-865 (1967).

29. Sessler, G., Acustica **8**, 395-397 (1958).

30. Parker, J. G., Adams, C. E. and Stavseth, R. M., J. Acoust. Soc. Am. **25**, 263-269 (1963).

31. Brekhovskikh, L. M., *Waves in Layered Media* (Academic Press, N. Y. 1960) p. 483 ff.

32. Seckler, B. D. and Keller, J. B., J. Acoust. Soc. Am. **31**, 192-216 (1959).

33. Kay, I. and Keller, J. B., J. App. Phys. **25**, 876-883 (1954).

34. Tolstoy, I. and Clay, C. S., *Ocean Acoustics* (McGraw-Hill, N.Y. 1966) Ch. 2.

35. Tolstoy, I., J. Acoust. Soc. Am. **37**, 1153-1155 (1965).

36. Barash, J., J. Acoust. Soc. Am. **43**, 378 (1968).

37. Wanner, J. C. L., Valee, J., Vivier, C. and Thery, C., J. Acoust. Soc. Am. **52**, 13 (1972).

38. Pierce, A. D. and Maglieri, D. J., J. Acoust. Soc. Am. **51**, 702-721 (1972).

39. Carlson, H. W., "Simplified Sonic-Boom Prediction," NASA Technical Paper 1122 (1978).

40. Grover, F. H., "A Survey of Atmospheric Wave Recordings at Blacknest," AWRE Report No. O 51/77 (1977).

41. Reed, J. W., private communication.

42. Zel'dovich, Y. B. and Raizer, Y. P., *Physics of Shockwaves and High-Temperature Hydrodynamic Phenomena* (Academic Press, N.Y. 1967) p. 852 ff.

43. Blackstock, D. T., "Nonlinear Acoustics," in *American Institute of Physics Handbook*, D. Gray Ed. (McGraw-Hill, N.Y., 1972).

44. Pestorius, F. M. and Williams, S. B., J. Acoust. Soc. Am. **55**, 1334-1335 (L) (1974).

45. Verniani, F., *Structure and Dynamics of the Upper Atmosphere* (Elsevier Scientific Publ. Co., N.Y. 1974) p. 27.

46. Lamb, H., *Hydrodynamics* (Dover, N.Y. 1945) p. 309.

47. Pierce, A. D., J. Acoust. Soc. Am. **44**, 1052-1061 (1968).

48. Crow, S. C., "Distortion of Sonic Bangs by Atmospheric Turbulence," J. Fluid Mech. **37**, 523-563 (1963).

49. George, A. R., "The Effects of Atmospheric Inhomogeneities on Sonic Boom," Third Conference of Sonic Boom Research, October 29-30, 1970, NASA-SP-255, 33-57 (1970).

50. Cole, N. J., and Friedman, M. B., "Analysis of the Multiple Scattering of Shock Waves by a Turbulent Atmosphere," Third Conference on Sonic Boom Research, October 29-30, 1970, NASA SP-225, 67-74 (1970).

51. George, A. R. and Plotkin, K. J., "Propagation of Sonic Booms and Other Weak Nonlinear Waves Through Turbulence," Phys. Fluids, **14**, 548-554 (1971).

DEPARTMENT OF THE NAVY

NAVAL RESEARCH LABORATORY
Washington, D.C. 20375

OFFICIAL BUSINESS
PENALTY FOR PRIVATE USE, $300
Third Class Mail

POSTAGE AND FEES PAID
DEPARTMENT OF THE NAVY
DoD-316